(1)

ELECTRON KINETIC STUDIES UTILIZING THE SOLUTION OF THE TIME DEPENDENT COLLISIONAL BOLTZMANN EQUATION

THESIS

[redacted]

[redacted]

AFIT/GEP/ENP/90M-[redacted]

DEPARTMENT OF THE AIR FORCE
AIR UNIVERSITY
AIR FORCE INSTITUTE OF TECHNOLOGY

Wright-Patterson Air Force Base, Ohio

AFIT/GEP/ENP/90D-1

ELECTRON KINETIC STUDIES UTILIZING THE SOLUTION OF THE TIME-DEPENDENT COLLISIONAL BOLTZMANN EQUATION

THESIS

William M. Hilbun
Captain, USAF

AFIT/GEP/ENP/90D-1

AFIT/GEP/ENP/90D-1

ELECTRON KINETIC STUDIES UTILIZING THE SOLUTION OF THE TIME-DEPENDENT COLLISIONAL BOLTZMANN EQUATION

THESIS

Presented to the Faculty of the School of Engineering

of the Air Force Institute of Technology

Air University

In Partial Fulfillment of the

Requirements for the Degree of

Master of Science in Engineering Physics

William M. Hilbun, B.S.
USAF
September 1990

Approved for public release; distribution unlimited

Preface

The purpose of this thesis was to examine electron kinetics in plasmas. The conditions encompass those relevant to the development of both excimer lasers and negative ion sources. The vehicle for this investigation was a numeric solution of the time-dependent collisional Boltzmann equation. The method of solution is based upon that developed by Rockwood (14). The processes considered in this code are elastic electron-neutral collisions, as well as ionization, excitation, attachment, and superelastic collisions.

Although much re-structuring and many program modifications and additions were required in order to study these devices and include these processes, the code's foundation was laid by Ges Seger. His programming style and foresight made it much easier for me to pick up where he left off. I also wish to thank my advisor, Dr William Bailey for his insight, help, and suggestions throughout this project. He even went as far as France in order to ask my questions of Dr Bretagne, another person that I am indebted to. His many articles on the subjects pertaining to plasma physics gave me further insight and ideas that proved useful.

Finally, I would like to thank my wife Kathi for her patience and support throughout this project, as well as staying up with me to the wee hours needlepointing beside my computer, just so we could be together.

Table of Contents

Preface ii

Table of Contents iii

List of Figures v

List of Tables vii

Table of Symbols viii

Abstract xi

I. Introduction 1

II. Background 6

- Origins of Solutions to the Boltzmann Equation 6
- Computational Method of Solution 7
- Electron-Electron Collisions 12
- Seger - A Working Code 13
- Transport Parameters 14
- Moments of the Boltzmann Equation 16
- External Sources 17

III. Theory 20

- Attachment 20
- Steady State Negative Mobility 22
- Electron-Electron Interactions 25
- Variable Energy Grid 28
- Electron Beams 33

IV. Computational Method 36

- Program Structure 36
- Energy Balance 40
- Transport Parameters 42

V. Analysis and Discussion 45

- Validation with Non-Uniform Energy Grid 45
  - Transport Parameters for Constant Collision Frequency 46
  - Transport Parameters for Gases 52
- Validation of Attachment Process 59
- Methods of Allocating Variable Energy Grids 63
- Electron-Electron Collisions with Non-Uniform Energy Grid 75
- Electron Beams 78
- Negative Total Electron Mobility 81

VI. Conclusion and Recommendations 86

Appendix A 89
Appendix B 96
Appendix C 101
Appendix D 105
Vita 111

List of Figures

1. Argon Momentum Transfer Cross Section 24
2. Energy Bin Allocation Function 30
3. He EDF at 4Td: Uniform vs Non-Uniform 49
4. Error in Numerical Calculation: Uniform vs Non-Uniform 50
5. EDF Calculated on Non-Uniform Grid for 300 K, E/N = 0 52
6. Ar Cross Sections 53
7. Ar Drift Velocity vs E/N (Td) 54
8. Ar Characteristic Energy vs E/N (Td) 55
9. Ar α/N vs E/N (Td) 56
10. H2 Cross Sections for M.T., Excitation, and Ionization 57
11. H2 Cross Sections for Ground State Vibrational Excitation 57
12. H2 Drift Velocity vs E/N (Td) 58
13. H2 2/3 <E> vs E/N (Td) 59
14. Ar EDF: Constant Attachment Frequency 61
15. Ar EDF: Increasing Attachment Frequency 62
16. Ar EDF: Decreasing Attachment Frequency 63
17. Rate Calculation Resulting in Over-Estimation 67
18. Rate Calculation Resulting in Under-Estimation 68
19. Dynamically Allocated Energy Grid 69
20. Non-Uniform Energy Axis with Validation Parameters 70
21. Allocation Function for 5 Td, n = 1.0 71
22. Allocation Function for 5 Td, n = 0.2 72
23. n vs % Error in Validation Parameters: 5 Td 73
24. n vs % Error in Validation Parameters: 4 Td 74
25. Allocation Function for 4 Td, n = 1.0 74

26. Allocation Function for 4 Td, n = 0.2 75
27. Electron-electron collisions only; Maxwellian initial vector 76
28. Electron-electron collisions only; Spike initial vector 77
29. H2 EDF with Electron Beam Source at 60.4 eV 79
30. H2 EDF with Electron Beam Source at 90.0 eV 81
31. Fluorine Cross Sections 82
32. Drift Velocity in Argon at Low E/N 83
33. EDF in Ar/F2 for 99.5%/0.5% Mix at 0.5 Td 84
34. Drift Velocity in Ar/F2 vs E/N 85
35. Energy Axis for Momentum Transfer 89
36. Sample Input File "input.com" for MEGABOLTZ 102
37. Sample Output File "test.dat" From MEGABOLTZ 104
38. Cross Section Data File for Argon 107

List of Tables

1. <E> for Constant Collision Frequency 47

2. Drift Velocity for Constant Collision Frequency 48

3. <E> for 0 Field and Constant Collision Frequency at 300 K 51

Table of Symbols

Symbol	Units	Description	Equation First Used
$\left(\frac{\partial f}{\partial t}\right)_{\text{collisions}}$		Phase space movement of electrons due to collisions	1
I		Identity Matrix	11
$<\varepsilon>$	eV	Average energy	15
$\vec{a}$	cm s^{-2}	electron acceleration	1
a_k	s^{-1}	Frequency with which electrons gain energy from external field and momentum transfer collisions	8
$\bar{a}_k$	s^{-1}	Frequency with which electrons gain energy from external field	53
$A_{k,l}$	$cm^3\ s^{-1}$	Excitation rate in ee collisions for electrons in k going to k+1 by electrons in l going to l-1	36
b_k	s^{-1}	Frequency with which electrons lose energy from external field and momentum transfer collisions	8
$\bar{b}_k$	s^{-1}	Frequency with which electrons lose energy from external field	53
$B_{k,l}$	$cm^3\ s^{-1}$	De-excitation rate in ee collisions for electrons going from k to k+1 by electrons going from l to l+1	36
C	s^{-1}	Rate matrix for all electron - neutral collisions	9
$\Delta\varepsilon_k$	eV	Width of energy bin k	33
$\delta\varepsilon_h$	eV	Threshold energy for inelastic process h	44
D_f	$cm^2\ s^{-1}$	Free Diffusion coefficient	14
E	V cm^{-1}	Electric Field	21
ε	eV	Electron energy	5
ε_k	eV	Characteristic electron energy	16
e	C	Electron charge	5
$\bar{\varepsilon}_k$	eV	Center of bin energy for bin k	49
f	$cm^{-3}\ eV^{-3/2}$	Reduced electron distribution function	1

f_o	$cm^{-3}\ eV^{-3/2}$	0^{th} order (symmetric) part of the spherical harmonic expansion of the distribution function	43
f_1	$cm^{-3}\ eV^{-3/2}$	1^{st} order (anisotropic) part of the spherical harmonic expansion of the distribution function	43
Δt	s	Time step used in numerical integration	10
dt	s	Differential time step used in integration	8
J_{ee}	$cm^{-3}\ s^{-1}$	Flux of electrons in energy space due to electron - electron collisions	4
J_{el}	$cm^{-3}\ s^{-1}$	Flux of electrons in energy space due to elastic electron - neutral collisions	4
J_f	$cm^{-3}\ s^{-1}$	Flux of electrons in energy space due to external fields	4
k		Bin number along energy axis	8
μ	$cm^2\ s^{-1}\ eV^{-1}$	Electron mobility	16
m	g	Electron mass	5
M_s	g	Molecular weight of neutral gas species s	6
m_{sj}		Integer representing the offset number of energy bins due to inelastic process j of gas species s	8
N	cm^{-3}	Neutral number density	5
n	cm^{-3}	Electron number density	3
ν	s^{-1}	Electron collision frequency	5
σ	cm^2	Cross section	5
q_s		Mole fraction	5
T	Kelvin	Gas Temperature	6
α	$\varepsilon^{1/2}cm^3s^{-1}$	Coefficient used in describing electron - electron collisions	7
R	$cm^3\ s^{-1}$	Kinetic rate of electron - neutral interaction	8
T	s^{-1}	Matrix describing electron - electron interactions	12
V_d	$cm\ s^{-1}$	Drift velocity	13
u	eV	Another way of writing energy	14
S	$cm^{-3}\ s^{-1}$	Source term of electrons	17
L	$cm^{-3}\ s^{-1}$	Loss term of electrons	17

J	Amps cm^{-2}	Electron current density	21
MT	eV cm^{-3} s^{-1}	Collective term describing energy losses due to momentum transfer	27
V	cm^3	Physical volume of the plasma	48
N^*	Unitless	Ratio of number of gas molecules in upper state to number in lower state	50
N_j	Unitless	Ratio of number of gas molecules in the lower state of process j to total number (ground state)	49
η_k	$cm^{-3}eV^{-1}$	Electron number density per unit energy in bin k	A-9

Abstract

In a continuing effort to analyze plasmas generated in a variety of ways, several refinements and improvements have been added to a numerical solution of the time-dependent collisional Boltzmann equation. The computational method utilized, originated by Seger (16) with the Rockwood formalism (14), includes elastic collisions, excitation, ionization, and superelastic collisions from multiple states, as well as electron attachment. The attachment process is explored, with the results confirming predictions made by the energy moment of the Boltzmann equation. The possibility of steady state negative mobility is explored in lean Ar/F_2 mixes, resulting in computational confirmation of theoretical predictions. A non-uniform energy grid is also incorporated into the method of solution, requiring new finite differenced representations for the electron flux terms from field, recoil, and electron-electron interactions. All of these terms are tested independently and validated against analytic results. Implementation, complete with inelastic collisions, is validated against experimental transport data for both molecular and rare gases. A method for dynamically allocating the energy grid in an effort to optimize the computation is developed and evaluated. The inclusion of the non-uniform grid results in the consideration of larger energy ranges than previously possible. This larger energy range, demonstrated up to 90 eV, allows the exploration of the effects of electron beams on the electron energy distribution. Energy distribution functions typical of a 10 A electron beam source are calculated at 60 and 90 eV and compared to previous solutions.

ELECTRON KINETIC STUDIES UTILIZING THE SOLUTION OF THE TIME-DEPENDENT COLLISIONAL BOLTZMANN EQUATION

I. Introduction

The Boltzmann equation is a continuity equation describing the flow of particles through phase space under the influence of externally applied forces and collisions. While analytic solutions to the Boltzmann equation exist for special cases, a quantitative analysis of plasma devices demands that the solution be obtained through the use of numerical methods. While some methods rely on finding only the steady state solution (8,10), a more general method is adapted. This admits the study of devices such as pulsed electron beam sustained plasmas, and permits self-consistent coupling of plasma chemistry and heavy particle kinetics. This time-dependent solution can be propagated forward in time, allowing the observation of the temporal evolution of the distribution, until either a steady state solution is achieved or a self-similar form of the distribution is obtained.

Solutions of the Boltzmann equation in energy space yield electron Energy Distribution Functions (EEDF). Once the EEDF is obtained, transport parameters and plasma kinetic rates can then be calculated by taking various moments of the distribution. These parameters and rates are invaluable in the design and optimization of many plasma devices. In gas-discharge lasers, a knowledge of the distribution function allows the kinetic pumping rates to be determined, which are a critical part of laser design and optimization. Since the plasma within such a device is gen-

erated and sustained by electron interactions with the electric field and gas particles, accurate pumping calculations are critically dependent on the proper treatment of all relevant collisional processes. Such processes include impact ionization, excitation, and superelastic collisions.

In excimer lasers and generators, ancilliary sources of ionization in the form of an electron beam or hot filament are employed. Beam energies in such devices are typically at much higher energies than the plasma mean energy. Therefore, the analysis of these devices requires not only the inclusion of a source term, but also an extension of the energy range in the solution method. In the exploration of the excimer lasers, and in particular the e- beam sustained rare gas halide lasers, the process of electron attachment is of fundamental importance, since it is just such a process that allows the production of the negative ions that are used in the reaction mechanism. Thus, any analysis of EEDFs characteristic of excimer lasers must properly include the process of electron attachment. The process of attachment is also of fundamental importance in discharges that contain a halogen gas as one of the constituents. These gases are very electronegative, and as such will tend to remove free electrons from the system. This electron loss can result in unusual effects within the discharge. One such effect leads to the possibility of a plasma discharge with a steady state negative total electron mobility. When an electric field is applied in a typical discharge, the electrons will tend to drift in a direction anti-parallel to the field. In such a case, the mobility is said to be positive. A negative mobility, therefore, leads to the electrons drifting parallel to the electric field. In such a case, it is possible for the electrons to give energy to the field, resulting in an increase in the field strength (15:1596).

The purpose of this study was to explore the electron processes fundamental to the operation of plasma devices that are of interest to the Air Force. These devices include electron-beam sustained plasmas, excimer lasers, and magnetic multicusp discharges. The analysis of each of these requires additional consideration within the code in terms of energy conservation, external sources, and electron interactions, both between themselves and with the gas particles. All of these processes will contribute to the steady state operating point of the plasma, and thereby have

a very large impact on the design, optimization, and analysis of the devices.

The analysis and understanding of the physics associated with these devices can be greatly improved by careful calculation of those properties which can be experimentally measured in the laboratory. If these calculated parameters compare favorably to the experimentally measured ones, then confidence can be given that all pertinent electron processes have been identified in the solution method. Such parameters include drift velocity, average energy, characteristic energy, and the ratio of the Townsend alpha coefficient to the neutral number density, α/N.

In the analysis of excimer lasers, multicusp discharges, and electron beams, a source of electrons is typically present at energies which are high compared to the energies typical of gas discharges. Therefore, in order to study such devices, the energy range of the solution must be extended to energies in the range of 0.1-100 keV. In the method of solution developed by Rockwood (14), this energy range is broken into K energy bins of equal size, and the method of finite differences utilized to solve the resulting K coupled equations simultaneously. This uniform energy method is practical in devices in which the energy range can be broken into approximately 300 energy bins or less. In the solution method, the K coupled equations are arranged into a square matrix of size K x K, and the inverse calculated. Aside from the physical limitation on the size of the K matrix due to computer memory, the time required for this inverse to be calculated is proportional to the cube of K (12:30-31, 33, 368), regardless of the method used. This requirement translates into a maximum energy range of approximately 30 eV for rare gases, and 15 eV or so for molecular gases. The number of energy bins required to accurately represent the distribution without rendering the basic assumption of finite differencing invalid is critically linked to the cross section's dependence on energy. In molecular gases, the inelastic processes that are grouped near the lower energies require a small energy bin size in order to accurately represent the distribution. This smaller bin size reduces the energy range of the solution for a fixed number of bins. In rare gases the threshold energy of the inelastic processes are higher,

and a larger bin size can generally be used before it leads to invalidating the finite differenced assumption. Clearly, then, this uniform bin size cannot be efficiently used to extend the energy range to that required by the e- beam devices.

In order to extend the present method of solution of the Boltzmann equation out to these higher energies, while still retaining accuracy and stability of the solution, several researchers have adopted a non-uniform energy grid, consisting of differential energy elements of unequal size (1:1201) (2:2209). One method used is to allocate the energy axis logarithmically (3:814). This method relies on the premise that the distribution changes most rapidly at the lower energies, and less so as the energy is increased. This method can be effective at calculating distributions out to the higher energies as Bretagne, et al (3) has done for molecular hydrogen, in which the inelastic thresholds are largely at the lower energies (1/2 to 12 eV). However, this method does not favor gases with inelastic processes which occur at higher energies, such as for the rare gases. This is because the differential energy elements are always increasing with energy, with no regard as to where an inelastic process begins. Since inelastic processes can lead to significant structure in the distribution, this method is not as desirable as one in which the energy element size is reduced in regions around the threshold energy.

While the non-uniform energy bin method is used to extend the energy range of the calculation, it may also prove to be more accurate than the uniform grid in the computation of the solution for a fixed energy range. Thus, if there is some method which can increase the accuracy of the solution in the same amount of time, then clearly it is advantageous to include this method into the code.

A computer code that yields the numerical solution to the time-dependent Boltzmann equation along a non-uniform energy grid has been developed using the formalism given by Rockwood (14), with the foundation established by Seger (16). This code considers excitation, ionization, attachment, elastic and superelastic processes as well as electron-electron interactions and momentum transfer. The possibility of excitation, ionization, and superelastic collisions

from multiple excited states is included. The transport parameters calculated with the distributions resulting from the non-uniform finite differenced representations of the field and recoil driven flux terms are validated against analytic results. The new finite differenced terms representing electron - electron collisions are tested for conservation of energy and particles, as well as for convergence to the proper form when considered alone. Using a logarithmically allocated energy grid, transport parameters for Ar and H_2 are compared to uniform grid calculations of the same, as well as experimental data. EEDFs for an electron beam generated H_2 plasma are calculated using a logarithmic energy grid and compared to previous calculations. A new method has been developed which allocates the energy axis based on the energy dependence of elastic and inelastic processes. The utility of this dynamic energy bin allocation method is explored using an approximate solution to the time independent Boltzmann equation as a benchmark distribution. In addition, the process of electron attachment is tested and validated with predictions made by the energy moment of the Boltzmann equation. The possibility of steady state negative mobility was studied in lean Ar/F_2 gas mixtures, with the results confirming theoretical predictions.

II. Background

Origins of Solutions to the Boltzmann Equation

The methods used to solve the Boltzmann equation for the distribution of electrons in energy space date back to 1946, with T. Holstein (8). Although his equations were derived for distributions driven by AC field conditions, they can be applied to the DC case as well. Holstein started with the Boltzmann equation describing the continuity of electrons in phase space:

$$\frac{\partial f}{\partial t} - (\vec{v} \cdot \nabla_r)f + (\vec{a} \cdot \nabla_v)f = \left(\frac{\partial f}{\partial t}\right)_{\text{collisions}} \tag{1}$$

where f is the electron distribution function describing the number of electrons in six dimensional phase space, thus $f = f(v_x, v_y, v_z, x, y, z, t)$, v is the electron velocity vector, **a** is the electron acceleration due to some applied force, ∇_r is the gradient in geometric coordinates, and ∇_v is the gradient in velocity coordinates. Holstein then assumed that the function f is very nearly spherically symmetric in velocity space for a sufficiently small applied field. This assumption allows the expansion of the distribution into an infinite series of spherical harmonics, with the axis defined by the direction of the field. Assuming azimuthal symmetry, the spherical harmonics move to Legendre polynomials:

$$f(x, v, \theta, t) = \sum_{n=0} f_n(x, v, t) P_n(\cos\theta) \tag{2}$$

where the P_n's are the Legendre polynomials. In practice, this infinite series is truncated after the first two terms, and is called the Lorentz, or P_1, approximation. The result of this expansion is a pair of coupled equations in terms of f_o and f_1, where the former represents the symmetric

part of the distribution, while the latter represents the anisotropic part. At this point, Holstein grouped the pair of coupled equations into a single equation. He then concentrated on finding the steady state solution to this single equation, which represents the solution to the Boltzmann equation for D.C. or high frequency A.C. discharges.

Computational Method of Solution

In 1973, Stephen Rockwood published a paper outlining a method used to calculate time dependent numerical solutions (14). In this method, the processes considered were electron-neutral elastic interactions, inelastic interactions in the form of excitation, ionization, and super-elastic collisions, as well as electron-electron collisions. The basic principle used to describe the time rate of change of the electron number density was the continuity equation. This equation can be written as

$$\frac{\partial n}{\partial t} + \nabla \cdot \mathrm{J} = \mathrm{S} - \mathrm{L} \tag{3}$$

where n is the number density of electrons, and $\nabla \cdot \mathrm{J}$ represents the flux of those electrons through energy space due to elastic and inelastic collisions as well as the external force arising from the electric field. S and L represent an external source and loss term respectively. Thus, the time rate of change of the electron number density due to elastic and inelastic collisions, as well as external forces can be written as a sum of terms expressing the divergence of the flux of electrons through energy space resulting from each process:

$$\frac{\partial n}{\partial t} = -\frac{\partial J_f}{\partial \varepsilon} - \frac{\partial J_{el}}{\partial \varepsilon} - \frac{\partial J_{ee}}{\partial t} + \left(\frac{\partial f}{\partial t}\right)_{collisions} + S - L \tag{4}$$

Here, the subscripts f, el, and ee denote the field, elastic, and electron - electron terms respectively. As Rockwood shows (14:2348), the current density of electrons in energy space due to the applied external electric field can be written as

$$J_f = \frac{2Ne^2(E/N)^2\varepsilon}{3m(\nu/N)}\left(\frac{n}{2\varepsilon} - \frac{\partial n}{\partial \varepsilon}\right)$$

$$\frac{\nu}{N} = \left(\frac{2\varepsilon}{m}\right)^{1/2} \sum_s q_s \sigma_s(\varepsilon) \tag{5}$$

where ν and $\sigma(\varepsilon)$ are the collision frequency and cross section for momentum transfer respectively, q_s is the mole fraction of species s, and n is the electron number density at energy ε.

Similarly, Rockwood shows that the current density of electrons in energy space due to elastic collisions with molecules of species s at a gas temperature of T is (14:2348)

$$J_{el} = \bar{\nu}\left[n\left(\frac{kT}{2} - \varepsilon\right) - kT\varepsilon\frac{\partial n}{\partial \varepsilon}\right] \tag{6}$$

$$\bar{\nu} = 2mN(2\varepsilon/m)^{1/2} \sum_s q_s \sigma_s(\varepsilon)/M_s$$

where M_s is the molecular weight of species s, and k is Boltzmann's constant. Note that in both of the expressions for the current densities J_f and J_{el} there is a term that is proportional to the number density of electrons n (convective), and another which is proportional to the energy gradient of the number density $\partial n/\partial \varepsilon$, (diffusive).

The remaining terms in the continuity (Boltzmann) equation are those which represent inelastic electron interactions with gas molecules and electron - electron interactions. The inelastic terms can be written classically as $n_e N\sigma(\varepsilon)v(\varepsilon)$, where the cross section σ would be for the appropriate inelastic process, N represents the number of collision partners, while n_e represents the number of electrons at the collision energy.

Intra-electron interactions can also be represented by the use of the Fokker-Planck approximation to the electron-electron collision integral described by the energy space divergence of the electron current density (14:2357):

$$\frac{\partial n}{\partial t}(\varepsilon,t) = -\frac{\partial J_{ee}}{\partial \varepsilon}$$

$$J_{ee} = \alpha\left[P\left(\frac{n}{2\varepsilon} - \frac{\partial n}{\partial \varepsilon} \right) - Qn \right] \tag{7}$$

where

$$P(\varepsilon,t) \equiv 2\varepsilon^{-1/2} \int_0^{\varepsilon} x n(x,t)dx$$

$$+ 2\varepsilon \int_{\varepsilon}^{\infty} x^{-1/2} n(x,t)dx$$

$$Q(\varepsilon,t) \equiv 3\varepsilon^{-1/2} \int_0^{\varepsilon} n(x,t)dx$$

Following the traditional method of solving differential equations by the method of finite differencing, Eq (4) is projected onto an energy axis that has been divided into K energy bins of, in general, various widths. Thus the differential equation is recast into K coupled linear equa-

tions and solved simultaneously. The actual derivation of the finite differenced terms representing the flux of electrons through energy space due to the applied electric field and elastic collisions between electrons and neutral gas molecules is included in Appendix A. In this derivation, particular attention has been paid to the fact that the energy axis is constructed of energy bins of various sizes, as well as maintaining numerical stability with no electric field present. Neglecting electron - electron collisions due to their non-linearity, and setting to zero the source and loss terms, the finite differenced Boltzmann equation can be written as (14:2349)

$$\frac{dn_k}{dt} = a_{k-1}n_{k-1} + b_{k+1}n_{k+1} - (a_k + b_k)n_k + \sum_{s,j} N_s(R_{sjk+m_{sj}}n_{k+m_{sj}} + R'_{sjk-m_{sj}}N_s^j/N_s$$

$$+R^i_{sk+m_{si}}n_{k+m_{si}} + \delta_{1k}\sum_m R^i_{sm}n_m - (R_{sjk} + R'_{sjk} + R^i_{sk})n_k) \qquad (8)$$

where k is the energy bin, s is the gas species, j identifies a particular inelastic process, and m is the threshold energy for that process. The R's represent rates $(\sigma(\epsilon)v(\epsilon))$ for each process. The a_k's and b_k's represent elastic promotions and demotions respectively, each from the k^{th} energy bin due to the applied field and recoil with heavy particles, while n_k represents the number density of electrons with energy between ϵ_{k-1} and ϵ_k. Therefore, n_k is a centered quantity in relation to the bin spacing. Thus the first term on the right represents the upflux of electrons due to momentum transfer and the external field from the energy bin directly below the k^{th} bin. Similarly, the second term represents the downflux of electrons due to momentum transfer and field from the energy bin directly above the k^{th} bin. The third term represents a loss of electrons out of the k^{th} bin due to the upflux of electrons to bin k+1, and downflux of electrons to bin k-1. The first term in the summation represents an addition of electrons to bin k due to an electron that underwent impact excitation at an energy level of k+m, where m represents the threshold energy for the excitation process. When that electron struck an atom and excited it to an upper level, it expended an energy equal to the excitation energy for that process. Thus, the electron lost an amount of energy equal to the threshold energy, thereby becoming an addition to the energy bin

that is located a "distance" of the threshold energy below it on the energy axis. The second term in the summation represents superelastic contributions to the k^{th} bin from the energy bin located a distance of the threshold energy below it. Likewise, the third term represents additions to bin k due to electrons causing impact ionization at bin k+m, where m represents the threshold for the ionization process. The next term reflects the assumption that all of the secondary electrons emitted by ionization reappear in the first energy bin on the axis. The last terms under the summation represent all the inelastic losses out of the k^{th} bin - excitation, superelastic, and ionization, respectively.

Recognizing that this differential equation was constructed so as to be linear in n_k, it can be rewritten in matrix form as

$$\frac{dn_k}{dt} = \sum_l C_{k,l} n_l \tag{9}$$

where C is a K x K matrix that remains constant with time, with K denoting the number of energy bins along the entire energy axis. The applied electric field and recoil terms will be placed into C such that it will become tridiagonal. The excitation and ionization terms will be placed into the C matrix above the diagonal, while the elements representing superelastic contributions will be placed below the diagonal. Thus, every element along the diagonal itself represents a loss out of the k^{th} bin, while every element not on the diagonal will represent an influx of electrons into the k^{th} bin.

The left hand side of Eq (9) can be differenced using a simple Euler relation:

$$\frac{dn_k}{dt} = \frac{n_k(t+\Delta t) - n_k(t)}{\Delta t} \tag{10}$$

Since the n_i on the right hand side of Eq (9) is the electron density at time $t + \Delta t$, Eq (9) can be rewritten as

$$\vec{n}(t + \Delta t) = (\mathrm{I} - \mathrm{C}\Delta t)^{-1}\vec{n}(t) \tag{11}$$

where I is the identity matrix, and $\vec{n}(t)$ represents the electron number density in each of the K energy bins at time t. From Eq (11), it can be seen that if the electron number density is known at any time t, it can easily be calculated for the time $t + \Delta t$. Since the C matrix is a constant, the inverse need be computed only once. Rockwood states that the convergence properties of this solution method are very good, even for arbitrary choices of $\vec{n}(0)$ (14:2349).

With the C matrix incorporating all of the electron-neutral collisional interactions, the single differential equation Eq (1) is broken into a number of coupled equations. This system of equations is then solved simultaneously, with the solution being given by the distribution function at the next time step. This solution is then marched forward in time, until the distribution changes very little in comparison to the previous solution. At such a point the self-similar form of the distribution has been achieved. This solution method has not, however, included the effects of electron-electron collisions in determining the final distribution. In the absence of any other processes, the electron-electron collisions will drive the distribution to a Maxwellian. The influence of this effect becomes more important at the higher fractional ionizations. However, since they are non-linear they cannot be included into the C matrix, but must be handled another way.

Electron-Electron Collisions

The electron-electron interactions are nonlinear with respect to n, thus they cannot be included into the C matrix of Eq (9). They are incorporated into the solution method by adding

to the right hand side of Eq (9) the matrix $T(\vec{n})$, which is tridiagonal. The resulting equation can be written as:

$$\vec{n}(t+\Delta t) = (I - C\Delta t)^{-1}(I + T\Delta t)\vec{n}(t) \qquad (12)$$

The elements within T directly correspond to the C matrix for the special case of momentum transfer only. The elements along the diagonal represent losses out of the bin, while the elements above and below the diagonal represent the downflux and upflux, respectively, of electrons from other bins. The primary difference between the two treatments lies in the fact that the coulomb collision integral takes the entire distribution of electrons into account at each time step in order to describe the electron interactions, which is the source of the nonlinearity. The momentum transfer between electrons and neutral particles, on the other hand, requires only a simple binary collision, thus they can be treated implicitly, while the former is treated explicitly in this approach. The elements of the T matrix must be computed for each time iteration throughout the computation. Appendix B contains the derivation of the finite differenced terms representing electron-electron interactions along the non-uniform energy axis. In this derivation, it is important to remember that the finite-differenced representation for the electron-electron interactions must obey three important principles: conservation of energy, conservation of particles, and relaxation of the distribution toward a Maxwellian when electron-electron collisions are the only process at work. Conservation of particles is ensured by the flux divergent form of the bin rate equations, coupled with appropriate boundary conditions. Conservation of energy is guaranteed by proper construction of the electron-electron matrices. The last property requires that with electron-electron interactions only, the distribution of particles should become a Maxwellian at a temperature equal to 2/3 of the average energy. This property is achieved by the use of detailed balance in requiring that the upflux of particles from one bin to the next higher bin equals the downflux from the higher bin to the one just below it.

Seger - A Working Code

Developed using the Rockwood formalism, Seger's code (16) was able to solve the Boltzmann equation for the self-similar form of the solution. In this method, the $\vec{n}(t + \Delta t)$ calculated by Eq (11) becomes the next $\vec{n}(t)$in the process. This code considered momentum transfer, superelastic, excitation, and ground state ionization processes. What was required of the user were input tables of cross section data for each process of each gas considered, the relative amount of each gas present, a particular E/N value, and certain other parameters which defined the problem to solve, such as neutral gas temperature and pressure, excited state population, etc. Once the solution to the Boltzmann equation was obtained, then drift velocity, average energy, and the free diffusion coefficient could be calculated.

Transport Parameters

The transport parameters serve to link the microscopic world to the macroscopic. In practice it is very difficult for the experimentalist to measure directly the distribution function itself, but it is very practical to measure other parameters which in theory depend directly on the distribution function. Conversely, the theoretician cannot directly determine any of the transport parameters, but must first calculate the distribution function upon which they are based. In order to determine if this distribution function is valid, the parameters calculated from it must be compared to the experimentally measured ones. In a very real sense then, the experimentalist is much like a blind man feeling different parts of the elephant in an effort to picture the whole beast.

The calculation of the transport parameters is based upon taking different moments of distribution function. The drift velocity is calculated by (10:472):

$$V_d = \frac{1}{3}\left(\frac{2e}{m}\right)^{1/2} \frac{\int_0^\infty f_1(u)u\,du}{\int_0^\infty f_o(u)u^{1/2}du} \tag{13}$$

where the two term approximation has been explicity retained in this expression. Thus, $f(u) = f_o(u) + f_1(u)\cos\theta$, where f_o and f_1 are the reduced distributions and are coupled to each other. The free diffusion coefficient D_f is calculated by (17:176):

$$D \equiv \overline{\left(\frac{u^2}{3\nu_r}\right)} \tag{14}$$

where u is the velocity, ν_r is the system relaxation collision frequency and is equal to the effective collision frequency when ν is independent of velocity (17:171-176). The average energy is calculated by taking the energy moment of the solution to the Boltzmann equation:

$$<\varepsilon> = \frac{\int_0^\infty \varepsilon f(\varepsilon)d\varepsilon}{\int_0^\infty f(\varepsilon)d\varepsilon} \tag{15}$$

The characteristic energy is a quantity which can be measured in an actual plasma discharge, and it can be used to define an equivalent Maxwellian temperature (4:101):

$$\varepsilon_k = \frac{eD}{\mu} = kT \tag{16}$$

Here, it has been written in terms of the Einstein relationship. It is seen that if the distribution was indeed Maxwellian, then the characteristic energy would be 2/3 of the average energy.

Moments of the Boltzmann Equation

Serving as another link between the unseen world of the very small and the world in which we live are the moments of the Boltzmann equation. Describing different aspects of the plasma, the moments of the Boltzmann equation detail the macroscopic quantities that researchers are able to measure. These are, principally, the production and loss of electrons, the velocity of electrons, and the energy of the electrons. The moments of the Boltzmann equation are generally written in terms of the averages which emphasize their macroscopic viewpoint.

The continuity equation has been mentioned previously in some detail, but will be written here in terms of the coordinate space divergence of the electron flux:

$$\frac{dn}{dt} = \nabla_r \cdot n\mathbf{v} + S - L \tag{17}$$

Assuming that the plasma is spatially homogeneous, and rewriting the production and loss terms as frequencies, Eq (17) becomes:

$$\frac{dn}{dt} = n_e(\nu_{ion} - \nu_{loss}) \tag{18}$$

The energy moment of the Boltzmann equation can be written as (4:111)

$$\frac{\partial n < \varepsilon >}{\partial t} + \nabla_r \cdot n < \mathbf{v}\varepsilon > - \vec{F} \cdot n < \mathbf{v} > = < \frac{d}{dt} n\varepsilon >_{coll} \tag{19}$$

where $\vec{F}$ is the force on the electron. The second term in this equation can be zeroed due to homogeneity. The first term can be expressed as two terms:

$$\frac{\partial}{\partial t} n <\varepsilon> \;=\; n\frac{\partial <\varepsilon>}{\partial t} + <\varepsilon>\frac{\partial n}{\partial t} \tag{20}$$

The third term in Eq (19) can be written as

$$\vec{F} n \cdot <v> \;=\; eEn \cdot <v> \;=\; J \cdot E \tag{21}$$

Using Eqs (18), (20), and (21) the energy moment of the Boltzmann equation takes the form

$$J \cdot E \;=\; M_{coll} + <\varepsilon> n(\nu_{ion} - \nu_{loss}) - n\frac{\partial <\varepsilon>}{\partial t} \tag{22}$$

When a self-similar form of the solution to the Boltzmann equation has been achieved through the iteration method previously outlined, the last term above will vanish. Thus, the power going into the discharge, $J \cdot E$, will be balanced by the sum of the inelastic and momentum transfer losses contained in the collision term (M_{coll}), along with the second term on the right hand side. This term represents the energy lost in bringing the secondary electrons produced in ionization up to the average energy of the distribution, as well as a correction factor caused by the loss of electrons through processes such as attachment, diffusion, and recombination.

Eq (22) proves to be very useful in describing the conservation of energy in the plasma discharge. This principle will serve as a chief diagnostic tool in determining whether each of the electron interactions considered is correctly incorporated into the solution method.

External Sources

In order to study the plasma within a hydrogen multicusp discharge, excimer laser, or electron beam assisted discharge, the external source of electrons must be included into the solution method of the Boltzmann equation. Following closely the work of Rockwood, A.E. Greene and C.J. Elliot (6) developed a very similar method of solution for the specific application of the electron beam pumped plasma of an excimer laser. In their development of the equations that describe the physics involved, they included the source term of the e- beam, as well as any loss terms that were considered (in this case, recombination was considered to be the dominate loss). In order to include these terms, reconsider Eq (3) with a non-zero source and loss term. Under such conditions, Eq (23) is iteratively solved until convergence.

$$\vec{n}(t+\Delta t) \quad = \quad (\mathrm{I}-\mathrm{C}\Delta t)^{-1}(\vec{n}(t)+\vec{\mathrm{S}}\Delta t) \tag{23}$$

The source term here represents the value of the source at each of the energy bins along the energy axis. For an electron beam with a sufficiently narrow energy spread, this vector will consist of zeroes everywhere except at the energy bin containing the e- beam.

In modeling a magnetic multicusp discharge in hydrogen, Bretagne (3), et al, has developed a code that also models a source term within a plasma. Their method of solution again follows that of Rockwood, with the inclusion of the source term and a loss term. The dominate electron loss processes in this case were assumed to be recombination and diffusion to the walls of the device. The solutions obtained by Bretagne were for the inclusion of an electron source at 90 eV in hydrogen. This is high when the mean electron energy is of the order of 5-10 eV.

In order to carry out the calculation of the distribution of electrons to these higher energies, Bretagne adopted a non-uniform differential energy element. In this scheme, the energy widths were allocated logarithmically, increasing with increasing energy. Using this method, it is assumed that the distribution changes most rapidly at the lower energies where the energy bin

widths are small, and less so at the higher energies where the bin widths are large. Ideally, what is required in a solution method is the allocation of a denser mesh of energy bins in the vicinity of inelastic process, since this is where the electron distribution will change most rapidly. This is due to the depleting effect that such a process imposes on the distribution as a result of the energy loss associated with the inelastic process. The energy loss of an electron involved in such a collision would be the threshold energy of the associated cross section.

While Bretagne's method could work well for hydrogen, in which most of the inelastic processes occur at energies which are relatively low (0.5 - 12 eV) compared to the energy of the source, it would seem to lack the flexibility needed to study other gases, such as the rare gases, in which inelastic processes can occur at energies of 20 eV or more (as in the case of Helium). In such a case, it may be possible for the energy bins to be too wide at these higher energies, thereby rendering invalid the basic assumption used in the finite differenced approach.

III. Theory

Having reviewed the theory behind the basic Boltzmann equation and the computational method utilized in determining its solution, the specific requirements of the plasma devices under consideration need to be addressed. These items are the processes of electron attachment and electron - electron collisions along a non-uniform energy grid, electron beams, and methods of dynamically allocating a non-uniform energy grid. In addition, the theory of steady state negative mobility is addressed.

Attachment

The process of electron attachment is very important in the study of certain plasma devices, particularly excimer lasers. These devices are at the forefront of technology in the efficient production of UV and near UV power (18:346). In electron beam pumped excimers, it is the attachment of electrons to the halogen that forms the negative ion used in the reaction process (18:348):

$$Ar^{+} + F^{-} + Ar \rightarrow (Ar^{+}F^{-})^{*} + Ar \qquad (24)$$

Thus, in e- beam pumped excimers, the process of attachment serves as an essential ingredient in the production of the excited state. However, this is not the case in discharge pumping (18:349):

$$Ar^{*} + F_2 \rightarrow (Ar^{+}F^{-})^{*} + F \qquad (25)$$

Here, the attachment process serves, at best, only as an auxiliary pumping channel. The benefits of the production of ionic Flourine are countered by the detachment process, which can lead to an unstable discharge, as pointed out by Verdeyen (18:349). So then, no matter what the pumping mechanism, electron attachment is an essential consideration in the analysis of the excimer laser.

The attachment process is taken into account by adding to the collision term of Eq (4) the attachment rate:

$$\frac{dn}{dt}\Big|_{attach} = -n_e N \nu(\varepsilon)\sigma_{attach}(\varepsilon) \tag{26}$$

This attachment rate can be easily incorporated into the finite differenced method of solution as part of the C matrix of Eq (9). The loss of electrons from the system involves a corresponding loss of energy. This energy loss, unlike those associated with ionization and excitation, is not associated with a fixed threshold value. Rather, the energy loss in the attachment process can be any energy within the domain of the attachment cross-section. The electron that undergoes attachment in energy bin k will lose an amount of energy equal to the center of bin energy for the k^{th} bin. Additionally, in order to achieve an energy balance once the steady-state (or self-similar) form of the solution has been established, a correction term for the electron loss must be taken into account, as shown in Eq (22).

Eq (22) can be rewritten slightly, showing explicitly the balance between the energy into the discharge and the various inelastic processes, along with momentum transfer losses:

$$J \cdot E = MT + (\langle \varepsilon_{ion} \nu_{ion} \rangle + \langle \varepsilon \rangle \nu_{ion}) +$$

$$(\langle \varepsilon_{loss} \nu_{loss} \rangle - \langle \varepsilon \rangle \nu_{loss}) + \langle \varepsilon_{exc} \nu_{exc} \rangle - \langle \varepsilon_{exc} \nu_{super} \rangle \tag{27}$$

Investigation into Eq (27) reveals several interesting cases. If the attachment frequency is constant, then the average energy of the electron distribution is exactly the same as if there were no attachment present. The presence of the constant attachment collision frequency would deplete a constant percentage of electrons from each energy, thus the form of the distribution would remain the same as if attachment were not present. The total number of electrons would, of course, be less with an attachment process.

Consider the case of an attachment frequency which increases with energy. Here, the attaching process would favor the high energy electrons over the slower ones, thus depleting the distribution at the higher energies. The result would be an EEDF with a lower average energy.

Finally, consider an attaching frequency which decreases with energy. In this case, the attachment process would tend to deplete electrons at the lower energies, resulting in a distribution which would have a higher mean energy than otherwise.

Steady State Negative Mobility

It is this last attachment case which forms the origin for the possibility of a plasma discharge with a negative steady state total electron mobility. In general, the mobility can be expressed as:

$$\mu = \frac{V_d}{E} \tag{28}$$

where E is the externally applied electric field, and v_d is the drift velocity. Using the classical two term spherical harmonic expansion with Eq (13) for the drift velocity, along with f_1 given by (10:471):

$$f_1 = -\frac{E}{N}\frac{\partial f_o}{\partial \varepsilon}\frac{1}{\sigma_m + \sum_h \sigma_h} \tag{29}$$

where σ_h is the inelastic cross section for process h, the mobility can be rewritten as (15:1594):

$$\mu = -\frac{1}{3}\sqrt{\frac{2}{m}}q\int_0^\infty \frac{\varepsilon}{N\sigma_m(\varepsilon)}\frac{df_o(\varepsilon)}{d\varepsilon}d\varepsilon \tag{30}$$

It has been assumed that the sum of the inelastic cross sections is much smaller than the cross section for momentum transfer. Eq (30) can be integrated by parts, with the integral term becoming:

$$\int_0^\infty \frac{\varepsilon}{\sigma_m}\frac{\partial f_o}{\partial \varepsilon}d\varepsilon = \frac{\varepsilon f_o}{\sigma_m}\Big|_0^\infty - \int_0^\infty f_o\left(\frac{1}{\sigma_m} - \frac{\varepsilon}{\sigma_m^2}\frac{\partial \sigma_m}{\partial \varepsilon}\right)d\varepsilon \tag{31}$$

The first term on the right hand side is zero. The evaluation of this term at infinity is zero due to the nature of the distribution function in that limit, and the evaluation at the lower limit is easily handled remembering that the cross section is finite at zero energy. Thus, a criteria for negative mobility is established:

$$\frac{d\sigma_m}{d\varepsilon} > \frac{\sigma(\varepsilon)}{\varepsilon} \tag{32}$$

Graphically, this criteria can be envisioned by drawing a line from the origin to the $\sigma_m(\varepsilon)$ at a particular energy (Figure 1). If the slope of the momentum transfer cross section at this energy is greater than the slope of the line drawn, then the criteria for negative mobility is met. It is seen that this criteria is met by Argon in the energy range of approximately 0.3 to 10.0 eV.

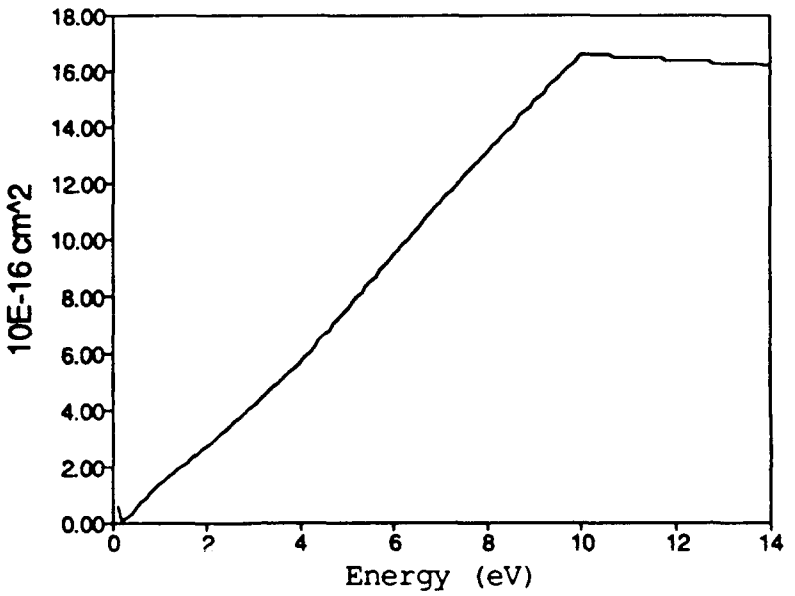

Figure 1. Ar momentum transfer cross section (21:1543)

An excellent description of the physical process at work in a discharge with a steady state negative mobility is given by Rozenburg, et al (15:1594). Briefly, however, it is the presence of an attaching cross section at low energies which can lead to the effect. If the electron distribution is shaped such that the majority of the integration of Eq (30) is carried out in the energy range over which Eq (32) is valid, then the mobility will be negative. Electrons travelling against the direction of the external electric field will tend to gain energy from the field. However, this energy gain will be transfered to the gas molecules through elastic collisions rather quickly, because the momentum transfer cross section increases rapidly with energy. Thus, these electrons will eventually end up with a velocity component in the direction of the field, at low fields. The electrons originally travelling in the same direction as the electric field will slow down due to the force of the field and will lose energy. If a large cross section for attachment is present at the lower energies, then there will be a large probability that the electron will be lost.

Additionally, since the electrons are slowing down, they will undergo fewer and fewer elastic collisions with the gas molecules, thus they will not tend to assume a spherical velocity distribution. These two processes will compete with one another, and conditions may be reached wherein the electrons will have a mean velocity component in the direction of the electric field, and therefore have a negative mobility.

Electron-Electron Interactions

The effect of electron-electron collisions in a plasma is to drive the distribution toward a Maxwellian (4:66). This effect is particularly important for discharges with high fractional ionization, and low E/N values (14:2350). Unlike the inelastic collisions that are incorporated into the C matrix of Eq (9), the electron-electron interactions are nonlinear and therefore time-dependent. Being described by the coulomb collision integral, the effect of a collision between electrons depends on the entire distribution of electrons in energy space. This nonlinear interaction is incorporated into the solution method by casting this collision integral into the energy space flux divergent formalism. In doing so, the two physical properties of conservation of particles and energy must be ensured. Additionally, the electron - electron collisions must tend to drive the distribution to a Maxwellian over time, reaching a Maxwellian in the steady state when only electron interactions are considered.

The recasting of the collision integral into the flux divergent formalism is accomplished by the following steps, and is developed in detail in Appendix B. Eq (7), which represents the Fokker-Planck approximation to the electron-electron collision integral, is finite differenced using a simple backward difference scheme. In doing so, the effect of the non-uniform energy axis is taken into account by defining the average electron number density between two adjacent bins as

$$n_{k+1/2} = \frac{\Delta\varepsilon_k n_{k+1} + \Delta\varepsilon_{k+1} n_k}{\Delta\varepsilon_k + \Delta\varepsilon_{k+1}} \tag{33}$$

while the term representing the energy space divergence of the electron number density becomes

$$\frac{\partial n_{k+1/2}}{\partial\varepsilon} = \frac{n_{k+1} - n_k}{\varepsilon_{k+1} - \varepsilon_k} \tag{34}$$

Notice that with constant energy bin widths, these representations will recover the usual expressions for the given quantities.

Next, the integrals contained in Eq (7) are replaced by summations over the entire energy range, and like terms of the electron number density are grouped together and expressed in the same formalism used previously to describe the field and elastic driven fluxes found in Eq (8). Eq (35) and Eq (36) result. $B_{k+1,l}$, the coefficient of n_{k+1}, represents the downflux of electrons going from energy bin k+1 to k by electrons going from bin l to l+1. The coefficient of n_{k-1}, which is $A_{k-1,l}$, represents the rate of upflux of electrons from k-1 to k, by electrons going from l to l-1.

$$\frac{\partial n_k}{\partial t} = a'_{k-1} n_{k-1} + b'_{k+1} n_{k+1} - (a'_k + b'_k) n_k \tag{35}$$

where the coefficients are expressed as:

$$a'_{k-1} = \sum_l A_{k-1,l} n_l \qquad b'_{k+1} = \sum_l B_{k+1,l} n_l \tag{36}$$

In order to ensure particle conservation, boundary conditions are applied to Eq (35) such that particles cannot be lost from the energy grid during the iteration process used to determine the solution. This condition, which requires that electrons cannot be demoted from the lowest energy bin, nor can they be excited from the highest energy bin, is expressed mathematically as:

$$A_{N,l} = B_{1,l} = 0 \quad \text{for all } l \in [l, N] \tag{37}$$

Energy conservation requires that

$$\frac{d}{dt}\int_0^\infty \varepsilon n(\varepsilon)d\varepsilon \;=\; \frac{d}{dt}\sum_{k=1}^{N} \varepsilon n_k \Delta\varepsilon_k \;=\; 0 \tag{38}$$

Carrying out the algebraic operations required in Eq (38) results in

$$B_{k,l} \;=\; \left(\frac{\Delta\varepsilon_{l+1} + \Delta\varepsilon_l}{\Delta\varepsilon_k + \Delta\varepsilon_{k-1}}\right) A_{l,k} \tag{39}$$

In the steady state with a Maxwellian distribution, the promotion and demotion interpretation for the $A_{k,l}$'s and $B_{k,l}$'s leads to the following balance between the two:

$$A_{k,l} n_k n_l \;=\; B_{k+1,l-1}\left(\frac{\varepsilon_l - \varepsilon_{l-1}}{\varepsilon_{k+1} - \varepsilon_k}\right) n_{k+1} n_{l-1} \tag{40}$$

This expression states that the rate of electron promotion from energy bin k to k+1 by electrons going from bin l to $l-1$ is balanced exactly by the rate of demotion of electrons from bin k+1 to k by electrons going from $l-1$ to l. Using Eq (38) and the expression for a Maxwellian energy distribution, Eq (40) can be expressed as:

$$A_{k,l} \;=\; A_{l-1,k+1}\left(\frac{\varepsilon_l - \varepsilon_{l-1}}{\varepsilon_{k+1} - \varepsilon_k}\right)\left(\frac{\varepsilon_{k+1}}{\varepsilon_k}\right)^{1/2}\left(\frac{\varepsilon_{l-1}}{\varepsilon_l}\right)^{1/2}$$
$$\times \exp\left[\frac{(\Delta\varepsilon_l + \Delta\varepsilon_{l-1}) - (\Delta\varepsilon_{k+1} - \Delta\varepsilon_k)}{2T}\right] \tag{41}$$

where T is the electron temperature. The proper construction of the A matrix will ensure that the distribution will be a Maxwellian in the steady state. The use of Eq (40) guarantees that energy will be conserved in the closed system, while the boundary conditions defined by Eq (38) will ensure the conservation of electrons.

Variable Energy Grid

The variable energy grid is envisioned as not only a method to increase the energy range of a calculation, but also as a means of increasing the accuracy of transport parameters and kinetic rates over the uniform grid. By increasing the number of energy bins, while holding the maximum energy constant, the finite differenced representation of the flux terms becomes a better approximation to reality, thus increasing the accuracy of the computed distribution to the actual distribution. In so doing, it is expected that the resultant transport parameters and kinetic rates computed from the distribution would also increase in accuracy. This trend has a practical limit however. As the width of the energy bin becomes sufficiently small, the computer roundoff error will begin to accumulate and result in significant deviations from the true values.

When considering a non-uniform energy grid, the question that naturally arises is how this mesh should be allocated. In the electron beam sustained plasma discharges, the logarithmically allocated axis has been used by Breiagne, which seems to be a useful method for H_2 and perhaps other molecular gases. However, it may not be the logical choice for gases with inelastic processes occurring at higher energies than those present in H_2 such as the rare gases. This is especially true if the ionization and excitation rates of such gases are of interest. Additionally, this method will indiscriminately allocate an energy axis with no regard as to the inelastic cross sections present. It would seem that the logarithmic method is used primarily for its ease of implementation.

A better method of allocation would logically take the inelastic cross sections and threshold energies into account. These inelastic processes would decrease the distribution very effectively at the threshold energies and beyond, thus the increased bin density at these energies would serve to increase the accuracy of the finite differenced representation of the differential equation. Since average energy and drift velocity are parameters that are mostly dependent on the bulk of the distribution, it is essential that the mesh used accurately calculates this region of the EDF. Additionally, excitation and ionization rates are parameters that mostly depend on the tail of the distribution, therefore it is important to be able to accurately calculate this portion of the EDF as well. The best possible mesh to calculate the former is clearly not the best to calculate the latter. The challenge is to be able to calculate both regions of the distribution with greater accuracy than a uniform mesh of equal grid points.

One method that can be used to define an energy grid has been used by Nickel (11:18) to calculate the radiation from various spectral lines. In his method, a function F is defined by the relation

$$F(\varepsilon) = \frac{\int_0^{\varepsilon} G(\varepsilon)d\varepsilon}{\int_0^{E_{max}} G(\varepsilon)d\varepsilon} \tag{42}$$

where G is some function yet to be determined, but which depends in this instance on the cross sections of the elastic and inelastic processes. Notice that the value of F can range between the limits of 0 and 1. The energy axis is divided into N equally spaced points, and the value of the function F is computed at each point. These points are then graphed versus energy as shown in Figure 2, where a 10 point uniform grid has been mapped onto a 10 point variable grid by using the Maxwellian distribution as the function G. The y axis, which ranges from 0 to 1, is also divided into N equally spaced points. Each of these points is then projected horizontally onto the

graph of F vs energy until intersection, and then down vertically to the energy axis. These intersections along the energy axis now define the new energy axis along which the solution to the Boltzmann equation will be computed. It is clearly seen from Eq (42) and figure 2 that in energy regions where the function G, and consequently function F, changes rapidly, the mesh of energy bins will increase. On the other hand, in regions where F changes little, few energy bins will be allocated. This is precisely the allocation scheme that is required, the only question being what does function G look like? Notice that if the function G were defined such that F was a straight line, then the mapping would be uniform to uniform.

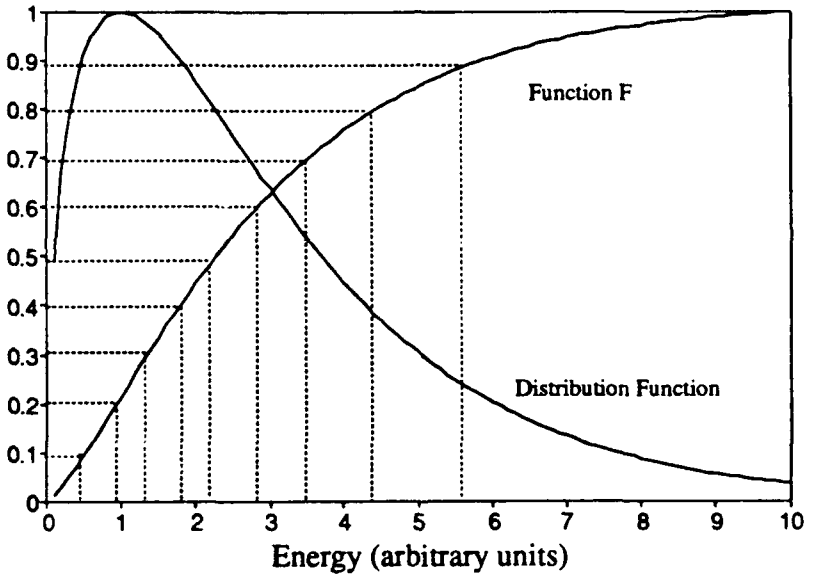

Figure 2. Maxwellian energy distribution with electron temperature of 2 units and the corresponding function F, where G is given by the number distribution

The choices of the function G can range from the electron distribution itself to some moment of the distribution, such as the energy moment. Unfortunately, these energy bin allocation functions require the distribution function itself, and this is the solution of the Boltzmann equation.

Thus these allocation choices require either first solving the Boltzmann equation on a uniform energy grid, and then re-solving it on the non-uniform grid, or accepting some assumptions that would allow the calculation of an approximation to the electron distribution quickly, without the need to iterate until convergence. The former choice is not ideal, due to the time requirements. Thus the latter alternative becomes the more attractive method.

Using the commonly accepted two term spherical harmonic expansion, the electron distribution can be represented as $f = f_o + f_1\cos(\theta)$, where f_o and f_1 are the solutions of a pair of coupled differential equations (10:471):

$$\frac{E/N}{3\varepsilon}\frac{\partial}{\partial\varepsilon}(\varepsilon f_1) + \sum_h Q_h f_o$$

$$= \frac{2m}{\varepsilon M}\frac{\partial}{\partial\varepsilon}(\varepsilon^2 Q_m f_o) + \sum_h Q_h(\varepsilon')f_o(\varepsilon')\left(\frac{\varepsilon'}{\varepsilon}\right) \tag{43a}$$

$$\frac{E}{N}\frac{\partial f_o}{\partial\varepsilon} + \left(Q_r + \sum_h Q_h\right)f_1 = 0 \tag{43b}$$

where Q is a cross section and $\varepsilon' = \varepsilon + \delta\varepsilon_h$. The subscript h denotes an inelastic process, while the subscript r denotes weighting each momentum transfer cross section by the mole fraction of the gas. The subscript m denotes the momentum transfer cross section weighted by mole fraction and molecular weight for the gas. Following Holstein's example (8:372), Eq (43a) is integrated with respect to energy, then Eq (43b) is substituted into Eq (43a), and again integrated with respect to energy. The pair of coupled differential equations now becomes a single implicit integral equation:

$$f_o(\varepsilon) = \exp[-\frac{3}{(E/N)^2}(\frac{2m}{M}\int_o^{\varepsilon} xQ_m(x)Q_t(x)dx$$

$$+\int_0^{\varepsilon}\frac{Q_t(x)}{xf_o(x)}\int_{\varepsilon}^{\varepsilon+\delta\varepsilon_h} Q_h(y)f_o(y)ydydx] \qquad (44)$$

where Q_t is the sum of all cross sections. Now, if some simplifying assumption can be made to eliminate f_o on the right hand side of Eq (44), then this function could be calculated quickly and may serve as a good choice to be used in Eq (42) in defining a non-uniform energy mesh. If it is assumed that f_o remains relatively constant over the interval ε to $\varepsilon + \Delta\varepsilon_h$, then this simplification will occur. The result is an equation for the electron energy distribution function which is a function only of energy, E/N, gas type, and the cross sections for the gas. Since these are all parameters that are known prior to the start of the numerical calculation of the solution to the Boltzmann equation, this function can be used quickly in defining a new energy grid through Eq (42).

Once the new energy grid has been established, and the solution to the Boltzmann equation computed along it, some criteria must be used by which the utility of the non-uniform method may be evaluated. Analytic solutions to the Boltzmann equation exist for the special cases of constant momentum transfer cross section and for constant momentum transfer collisional frequency. In both of these cases, any inelastic cross section, Q_h, has been zeroed out. Therefore the double integral on the right hand side of Eq (44) vanishes. The remaining integral can be handled analytically, allowing calculation of such parameters as average energy and drift velocity through the use Eq (15) and Eq (13) respectively. Therefore, in these cases, the average energy and drift velocity calculated using uniform and non-uniform energy grids can be compared to the analytically determined ones. However, since the primary utility of the non-uniform energy grid most likely lies in the case of when inelastic cross sections are included, the

analytic calculation of these parameters is precluded. In this case, a good figure of merit is a calculation of the parameters carried out using a uniform energy grid consisting of a sufficient number of points such that the calculated parameters do not change much.

Electron Beams

Electron beams can be included into the method of solution by returning to Eq (9). If the source and loss terms in Eq (3) are non-zero, then Eq (9) becomes:

$$\frac{dn_k}{dt} = \sum_l C_{k,l} n_l + S - L \tag{45}$$

where the units of the source term S and loss term L would be $cm^{-3}s^{-1}$. Applying Euler's formula for the derivative and solving for $n(t + \Delta t)$, the following is obtained:

$$\vec{n}(t + \Delta t) = (I - C\Delta t)^{-1} \{(S - L)\Delta t + \vec{n}(t)\} \tag{46}$$

The solution to the Boltzmann equation is found at each time interval $t + \Delta t$, and the self-similar solution is found by iterating Eq (46) until the programmed convergence criteria is met.

In analyzing the effect of only the e- beam on the distribution, it is desirable to zero the electric field. Doing so with the finite differenced equations used in previous codes created numerical instabilities arising from the recoil flux term, J_{el} (6:2948). In those representations for the flux, the reduction of the electric field below some minimum value allowed promotion and demotion rate coefficients (a_k's and b_k's) that were almost all negative at some values of energy. With no forces acting on the closed system of electrons, what is required of the electron energy

distribution is to obtain a Maxwellian whose average energy is 1.5 times the gas temperature. The finite differenced representation for the recoil flux divergent term as achieved in Appendix A preserves this property, thus maintaining numerical stability over a range of temperatures.

The source term S can be written as

$$S = \frac{I}{Ve} \tag{47}$$

where V is the plasma volume, and I is the current at the source energy. Eq (47) is written for a point source in energy. If a source is used that is broad in relation to the energy bins around it, then this term would need to be spread out into several bins.

The addition of the electron beam source also requires its inclusion into the energy balance equation Eq (22), where now the J • E term is replaced (or augmented) by the power into the discharge by the e- beam, namely:

$$P_{e\text{- beam}} = \frac{I}{Ve}\varepsilon_{beam} \tag{48}$$

where the units of this power term are $eVs^{-1}cm^{-3}$, a power density.

The effect of having a source of electrons at a high energy is to produce ionization and excitation of the gas molecules. These processes all constitute losses of energy for the source electrons, thus they will be displaced down to the lower energies by an amount equal to the threshold energy of the process. If the source is at large enough energies, these electrons can be displaced along the energy grid many times before elastic collisions with the gas become dominate. The interactions between the ionizing electrons and the secondary electrons produced during ionization gives rise to what Bretagne (1:1119) calls energy sharing. In the present Boltzmann code, the secondary electrons are all assumed to appear at the lowest energy bin, while in reality some

energy is shared between it and the ionizing electron, resulting in some secondary electrons appearing at higher energies. This energy sharing tends to smooth the distribution when compared to the classical treatment of ionization that neglects it. However, according to Bretagne, this classical treatment of the ionization process can be used to accurately model the electron beam sustained discharge as long as 1) low energy inelastic process are not dominate and 2) the energy of the source is not too high (ε_p < about 100 eV) (1:1201). The first condition can readily be met in the rare gases, however in molecular gases care must be taken to ensure that this is true.

IV. Computational Method

Program Structure

The Boltzmann code developed, Megaboltz, solves the time-dependent Boltzmann equation. Output consists of the EEDF, the kinetic rates for the inelastic processes considered, and the transport parameters. An energy balance, which is the primary compututational diagnostic, is also a monitored output. A user's guide to the code is included in Appendix C, however the principal routines will be briefly outlined in this section.

The user can select from a menu regarding the type and amount of each gas present in the plasma, the electric field to neutral number density ratio (E/N), the gas temperature, pressure, and electron number density. Additionally, the user can choose to see or plot the interpolated cross sections for any of the kinetic processes, as well as turn on/off the electron-electron collisions and electron beam. The source energy of the electron beam is also set by the user on the menu. Finally, the energy grid is selected, whereby the number of energy bins along the energy axis and the maximum energy are defined. This grid can be constructed in a number of ways: uniformally, logarithmically, or dynamically. When the energy grid is constructed dynamically, the elastic and inelastic cross sections will have some influence on the location and density of the energy bins.

The value of the independent variable used in the numerical integration of the Boltzmann equation is also set in "input.com". This number represents the time step of integration used in Eq (11) and Eq (12), and would typically be at least as small as the time scale for the dominate electron collisional process.

In order to properly invoke the code, the user must define the physical situation of interest. This is done by editing the file called "input.com". This file will be read when the program is run, thus it must be edited before starting the program. This file defines the basic problem to be solved.

After the input file "input.com" is read, the code will look for the cross section files of the gases that were selected. These cross section files are external to the code, and they must be formatted according to Appendix D. These files contain cross section vs energy data stored as tables, along with some other required information. For each type of inelastic process, a number called NSTATE is read, which tells the code the ratio of the gas molecules that are in the lower state of the process the cross section represents to the total number of gas molecules. Excitation or ionization from the ground state would have NSTATE values of 1.0. An excitation from some excited state to a higher state would have an NSTATE value of between 0.0 and 1.0. By assigning each process a separate NSTATE value, any of the inelastic processes may be turned on or off. For excitation processes, an additional variable is read which defines the ratio of the molecules in the upper excited state to the number in the lower state, which may or may not be the ground state. This value, NSTAR, is used to compute the superelastic rates.

Once all of the gas cross sections are read in, the energy axis is defined according to the user's choice in "input.com", and the elastic and inelastic cross sections are interpolated from the data tables at each energy point. Next, the matrix C as used in Eq (9) is constructed. The elements of this matrix include all excitation, ionization, superelastic and attachment processes. Each element has units of s^{-1}, and is determined by how the particular process effects the flow of electrons in energy space at each bin energy. Since the number density of electrons, n_k, is a quantity that is defined at the center of energy bin k, the coefficients of n_k are also constructed to be center of bin values.

Impact excitation and ionization will cause an electron with energy $\varepsilon > \Delta\varepsilon_{thresh}$ to lose an amount of energy equal to this threshold value. Thus, an electron will be lost out of the higher energy bin, reappearing at the bin corresponding to $\varepsilon - \Delta\varepsilon_{thresh}$, as outlined by Eq (49).

$$C_{k,k+m_j} = \sum_{s,j} N_s N_j \sigma\left(\bar{\varepsilon}_{k+m_j}\right) V\left(\bar{\varepsilon}_{k+m_j}\right)$$

$$C_{k,k} = -N_s N_j \sigma(\bar{\varepsilon}_k) V(\bar{\varepsilon}_k) \tag{49}$$

where s is the gas type, j is the process, k represents the energy bin, m_j is the bin offset corresponding to a threshold energy of $\Delta\varepsilon_j$. N_j is the NSTATE value for process j, and N_s is the number density of gas molecules for gas type s. The center of bin energy value for bin k is expressed as $\bar{\varepsilon}_k$. The first term on the right hand side represents gains into bin k due to electrons undergoing collisions at energy k+m, while the second term represents excitation losses out of bin k.

Superelastic collisions are handled similarly, except now the addition of electrons at energy ε are from energy $\varepsilon - \Delta\varepsilon_j$. The electron undergoing a superelastic collision at energy ε will be sent to $\varepsilon + \Delta\varepsilon_j$. The superelastic matrix elements are assigned by

$$C_{k,k-m_j} = N^* N_s \left(\frac{\bar{\varepsilon}_k}{\bar{\varepsilon}_k - \Delta\varepsilon_j} \right) \sigma(\bar{\varepsilon}_k) V(\bar{\varepsilon}_k - \Delta\varepsilon_j)$$

$$C_{k,k} = -N^* N_s \left(\frac{\bar{\varepsilon}_k + \Delta\varepsilon_j}{\bar{\varepsilon}_k} \right) \sigma(\bar{\varepsilon}_k + \Delta\varepsilon_j) V(\bar{\varepsilon}_k) \tag{50}$$

where $k - m_j$ is the energy bin corresponding to $\varepsilon_k - \Delta\varepsilon_j$, and detailed balance has been used to express the superelastic cross section in terms of the excitation cross section.

In the process of attachment, the electron is lost from the system - they do not reappear anywhere so far as the energy distribution is concerned. This loss of electrons is assigned to elements in C by

$$C_{k,k} = -N_g N_{state} \sigma(\bar{\varepsilon}_k) V(\bar{\varepsilon}_k) \tag{51}$$

Once all of the processes have been loaded into the C matrix, the inverse of the (I-Cdt) is calculated. In the present version of the code, this matrix inversion is carried out by the IMSL v. 9.2 library routine LUDATF. This routine performs the matrix inversion using the L-U decomposition method (12:31). As is reported by Seger (16:16) and Honey (9:118), L-U decomposition is generally preferable to other methods such as Gauss-Jordon, Gauss-Seidel, and successive over relaxation (SOR) in terms of both speed and accuracy. In the L-U decomposition method, the inverted matrix is actually two matrices, one upper triangular (U) and the other lower triangular (L), stored as a single matrix. The new $\vec{n}(t+\Delta t)$ vector must be computed by forward substitution with the L matrix, and then back-solving with the U matrix. Once the $(I - C\Delta t)$ matrix is triangularized, which only needs to be done once, then the forward/backward substitution is carried out fairly quickly.

Each time the new $\vec{n}(t+\Delta t)$ vector is computed, it is tested for convergence with the previous vector, $\vec{n}(t)$. This convergence test is accomplished at each energy value, and each number density vector is normalized to its respective total electron number density. Once the convergence test is passed, or if the maximum number of iterations is reached, the last $\vec{n}(t+\Delta t)$ vector computed is passed to a routine which calculates the excitation, ionization, superelastic, and attachment rates. These rates are calculated by

$$R = \frac{\int_0^\infty n_e(\varepsilon)\sigma(\varepsilon)V(\varepsilon)d\varepsilon}{\int_0^\infty n_e d\varepsilon}$$

$$= \frac{\sum_{k=1}^{N} n_k \sigma(\bar{\varepsilon}_k)V(\bar{\varepsilon}_k)}{n_{e_{tot}}} \qquad (52)$$

where the units on the rates are cm^3/s.

Energy Balance

When the rates have been calculated, the final electron distribution is passed off to the energy balance routine. This routine computes the energy into the discharge, and the energy losses from all elastic and inelastic processes. The balance of energy inputs with loss mechanisms serves as a primary computational diagnostic for the acceptance of any data run. The energy sources consist of the electric field and/or the electron beam. The electric field's energy contribution into the discharge is just J • E. This can be written as

$$\frac{dE}{dt} = \sum_k (\bar{a}_k \Delta\varepsilon_k - \bar{b}_k \Delta\varepsilon_{k-1}) n_k \qquad (53)$$

where $\bar{a}_k$ represents the flux of electrons through energy space from energy ε_k to energy ε_{k+1} due to the applied field, and defined as in Appendix A. Similarly, $\bar{b}_k$ represents the flux of electrons from ε_k to ε_{k-1} due to the applied field. The separate $\Delta\varepsilon_k$'s illustrate the effect of the non-uniform energy axis. The first term reflects the energy gained by electrons which have velocity components anti-parallel to the electric field, therefore accelerating to higher velocities. The $\bar{b}_k$

term reflects the slowing down of the electrons which have some velocity component in the same direction as the field. If more electrons speed up than slow down, then the field will have a net positive input of power into the discharge. If more electrons slow down, then the field will gain energy from the electrons. This last case is predicted from the effects of a large attachment cross section at low energy, and a momentum transfer cross section that increases with energy (15:1596). The energy into the discharge is given by Eq (53).

The energy losses consist of elastic and inelastic collisions. The rate of energy lost in the elastic collisions can be written as

$$\frac{dE}{dt}\Big|_{el} = -\sum_k [(a_k - \bar{a}_k)\Delta\varepsilon_k - (b_k - \bar{b}_k)\Delta\varepsilon_{k-1}]n_k \tag{54}$$

The excitation loss is expressed as

$$\frac{dE}{dt}\Big|_{exc} = -\sum_{s,j,k} N_s N_j n_k \sigma_j(\bar{\varepsilon}_k) V(\bar{\varepsilon}_k) \Delta\varepsilon_{s,j} \tag{55}$$

where $\Delta\varepsilon$ is the excitation energy threshold for process j of gas s and N_j is the ratio of the number density of gas molecules in the lower state of process j to the number density in the ground state. Thus, for ground state excitation this number would be 1.0, whereas for excitation from some excited state it would less that 1.0. The ionization energy loss is similar to the excitation loss, with the additional term reflecting the energy lost in bringing all the secondary electrons up to the average energy of the distribution. It is expressed as

$$\left.\frac{dE}{dt}\right|_{ion} = -\sum_{s,j,k} N_s N_j n_k \sigma_j(\bar{\varepsilon}_k) V(\bar{\varepsilon}_k) \Delta\varepsilon_{s,j} - \frac{\sum_k \bar{\varepsilon}_k n_k}{\sum_k n_k} \sum_{s,j,k} N_s N_j \sigma_j(\bar{\varepsilon}_k) V(\bar{\varepsilon}_k) n_k \quad (56)$$

where the second rate sum is carried out over all ionization processes j.

The superelastic loss is really an energy gain, and can be written as

$$\left.\frac{dE}{dt}\right|_{super} = \sum_{s,j,k} N_s N_j N^* n_k \left(\frac{\bar{\varepsilon}_k + \Delta\varepsilon_{s,j}}{\bar{\varepsilon}_k}\right) \sigma_{exc}(\bar{\varepsilon}_k + \Delta\varepsilon_{s,j}) V(\bar{\varepsilon}_k) \Delta\varepsilon_{s,j} \quad (57)$$

where the product $N_s N_{state} N^*$ is simply the number of molecules in the excited state of process j belonging to gas s.

The attachment energy loss is

$$\left.\frac{dE}{dt}\right|_{attach} = -\sum_{s,j,k} N_s N_j n_k \sigma(\bar{\varepsilon}_k) V(\bar{\varepsilon}_k) \bar{\varepsilon}_k + \frac{\sum_k \bar{\varepsilon}_k n_k}{\sum_k n_k} \sum_{s,j,k} N_s N_j n_k \sigma_j(\bar{\varepsilon}_k) V(\bar{\varepsilon}_k) \quad (58)$$

where the second rate sum is carried out over all attachment processes j. The second term in Eq (58) represents the correction to the energy lost in attachment due to loss of electrons, as Eq (22) suggests.

Transport Parameters

The calculation of the transport parameters is accomplished after MEGABOLTZ computes the energy balance. These parameters are drift velocity, average energy, characteristic energy, and the free diffusion coefficient. The drift velocity Eq (13) can be expressed in terms of the rate of energy gained by the electrons from the electric field (14:2350):

$$v_d = \frac{\dot{E}_g}{E \sum_k n_k} \tag{59}$$

where $\dot{E}_g$ was calculated in Eq (53) as part of the energy balance. The diffusion coefficient is calculated with Eq (14) as

$$D_f = \frac{1}{3}\left(\frac{2}{m}\right)^{1/2} \sum_k \frac{\bar{\varepsilon}_k f_k \Delta\varepsilon_k}{\sum_s q_s \sigma_s(\bar{\varepsilon}_k)}$$

$$\text{where} \quad f_k = \frac{n_k}{\bar{\varepsilon}_k^{1/2} \Delta\varepsilon_k \sum_k n_k} \tag{60}$$

Once the drift velocity and diffusion coefficient are calculated, then the characteristic energy can be calculated by Eq (16), which can be expressed as

$$\varepsilon_k = \frac{E D_f}{v_d} \tag{61}$$

since $\mu = v_d/E$.

The average energy is calculated by

$$<E> = \frac{\sum_k \bar{\varepsilon}_k n_k}{\sum_k n_k} \tag{62}$$

Once these parameters are calculated, they can be compared to experimental data. Very often, it is through just such a comparison that a particular gas' cross section that is unknown in some energy range is refined or even defined altogether. It is these transport parameters that link the distribution function to observables in the real world.

V. Analysis and Discussion

Validation with Non-Uniform Energy Grid

The extension of the energy range of the solution is critical in being able to include sources of electrons in the computation of the distribution function. This energy extension involved re-deriving the field and recoil electron flux terms for a non-uniform energy grid. Several methods were used in order to validate the Boltzmann code with the non-uniform energy mesh. First, calculations of <E> and ν_d using a non-uniform grid were compared to calculations using a uniform grid for the case of no inelastic processes and $\nu_{M.T.}$ =constant. Since analytic solutions to the Boltzmann equation exist for the case of $\nu_{M.T.}$ = const, these parameters could then be compared to the expected analytic values. Secondly, ε_{char}, ν_d, and α/N were calculated on both the uniform and non-uniform energy grids and compared to experimental data for several gases, both molecular and rare. Finally, with the electric field turned off, the new finite differenced representation for the momentum transfer recoil term (Eq (A-17a) and Eq (A-17b)) was tested for convergence to the proper value of <E> for several gas temperatures.

In the validation of the non-uniform energy grid, some method must be used whereby the grid is allocated. For this analysis, the non-uniform grid was established by using a pseudo-logarithmic method. This method defines the width of each energy bin by the relation

$$\Delta\varepsilon_k = \mathrm{Ln}(k)^{\alpha} + \mathrm{E}_{min} \qquad (63)$$

where the variables E_{min} and α were defined so that the maximum energy of the non-uniform energy grid was approximately the same as the maximum energy of the uniform grid. Thus, the

energy at each bin of the non-uniform grid was established by summing the width of each bin below it. When any comparisons were made between transport parameters calculated using the uniform and variable energy grids, the number of energy bins used in each method was constant.

Transport Parameters for Constant Collision Frequency

Since an analytic solution to the Boltzmann equation exists for the special case of a constant momentum transfer collision frequency, this condition was used in order to compare the calculated average energy and drift velocity to the analytically determined ones. The analytic values of <E> and v_d were determined by using Eq (44) with $\nu_{M.T.} = 3.05 \times 10^{12} s^{-1}$ and no inelastic cross sections in order to derive the reduced electron distribution function, $f_o(\varepsilon)$. From this function, the average energy can be determined by Eq (15). The drift velocity is determined by using $f_o(\varepsilon)$ in Eq (44b) to get $f_1(\varepsilon)$, from which v_d is calculated by Eq (13). The analytic expressions derived as a result are

$$< E > = 4.1318 \times 10^{-2} (E/N)^2 \quad eV \tag{64a}$$

$$v_d = 1.412 \times 10^5 (E/N) \quad cm/s \tag{64b}$$

Table 1 shows the comparisons between <E> calculated with a uniform and variable mesh to the analytic values. The energy axis was divided into 150 bins, with the maximum energy varying from 2 eV at 2 Td, to 200 eV at 20 Td. For the variable energy mesh, Emin and α were varied so that the maximum energy was approximately the same as in the uniform case. The maximum energy for the calculation was determined by requiring at least a six order of magnitude drop in the distribution at the maximum energy, but not more than a ten order of magnitude decrease. Limiting the drop to less than ten orders of magnitude will prevent any numerical

errors arising from computer roundoff. Requiring at least a six order of magnitude drop will ensure that nearly all of the electrons are accounted for in the calculation of the transport parameters.

Table 1

<E> (eV) for $\nu_{M.T.}$ = Constant, Calculated for Uniform vs Non-Uniform Energy Grid

E/N (Td)	Analytic	Uniform	% Error	Non-Uniform	% Error
2	0.165	0.166	0.606	0.167	1.212
4	0.662	0.665	0.453	0.667	0.755
6	1.487	1.489	0.135	1.494	0.471
8	2.644	2.651	0.265	2.658	0.530
10	4.132	4.155	0.557	4.168	0.871
12	5.950	5.983	0.555	6.003	0.891
14	8.098	8.139	0.506	8.174	0.939
16	10.577	10.630	0.501	10.680	0.974
18	13.387	13.460	0.545	13.510	0.919
20	16.527	16.610	0.502	16.680	0.926

In every case, the code has over-estimated the average energy. The values calculated with the non-uniform axis are consistently higher than those calculated with a uniform grid. However, it

must be remembered that the variable energy grid used in these calculations has been somewhat arbitrarily constructed; that is, each energy bin width was assigned according to Eq (63). No attempt was made to optimize the grid for the calculations of drift velcity or average energy.

Table 2 shows a similar comparison between the drift velocity calculations with the different energy grids compared to the analytic values for different E/N values. The calculations at each E/N were accomplished using the same grid mesh that was used previously in the <E> calculations.

Table 2

V_d ($\times 10^6$ cm/s) for $\nu_{M.T.}$ = Constant, Calculated for Uniform vs Non-Uniform Energy Grid

E/N (Td)	Analytic	Uniform	% Error	Non-Uniform	% Error
2	0.2824	0.2817	0.248	0.2813	0.390
4	0.5648	0.5633	0.266	0.5617	0.549
6	0.8472	0.8413	0.696	0.8413	0.696
8	1.1296	1.124	0.496	1.123	0.584
10	1.4120	1.409	0.212	1.406	0.425
12	1.6944	1.691	0.200	1.687	0.437
14	1.9768	1.971	0.293	1.966	0.546
16	2.2592	2.253	0.274	2.248	0.496
18	2.5416	2.535	0.297	2.529	0.496

The calculated results were consistently under-estimating the analytic values, with the uniform grid generally giving better estimations of the velocities than the non-uniform grid. Again, no effort was made to construct an optimized energy grid is this case.

Figure 3 shows a comparison between the energy distributions calculated for the uniform and non-uniform grids and the analytic distribution for an E/N of 4 Td. The electron distributions have been plotted as a reduced distribution ($cm^{-3}eV^{-3/2}$) such that a Maxwellian will appear as a straight line when plotted on a semi-logarithmic scale. Plotted on this scale, there is very little difference between each of the distributions. The dotted line represents the distribution calculated on the non-uniform grid, while the solid line represents the uniform grid calculation. The dashed line represents the analytic distribution calculated under the identical conditions. Both of the calculated distributions over-estimate the analytic distribution slightly, illustrating the over-estimation of the average energy.

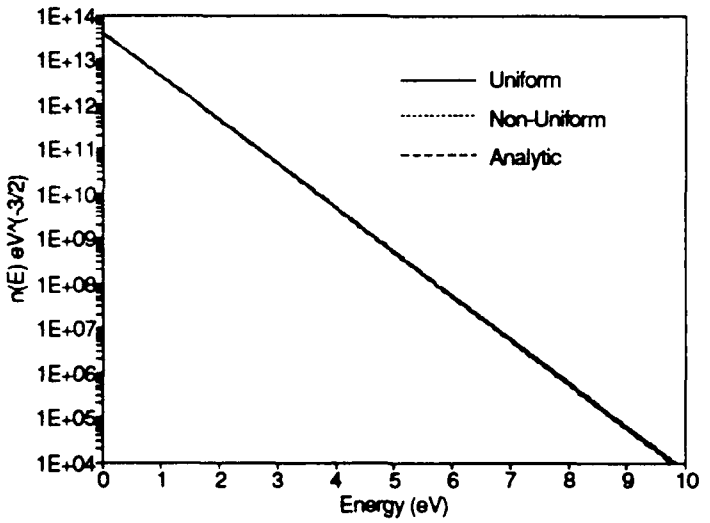

Figure 3. He EDF at 4 Td: Uniform vs Non-Uniform

Figure 4 shows the percent error in the two calculated distributions as a function of energy. This error is defined as $(f_{analytic} - f_{numeric})/f_{analytic} \times 100$.

An over-estimation of the correct number density will result in a negative error, while an under-estimation will result in a positive error. At low energies, the non-uniform grid results in over-estimating the correct values, while the uniform grid under-estimates the correct values. At larger energies, both of the calculated distributions over-estimate the analytic result. In this region, the non-uniform grid over-estimates the analytic distribution more than the uniform grid, leading to a greater calculated average energy for the former compared to the latter.

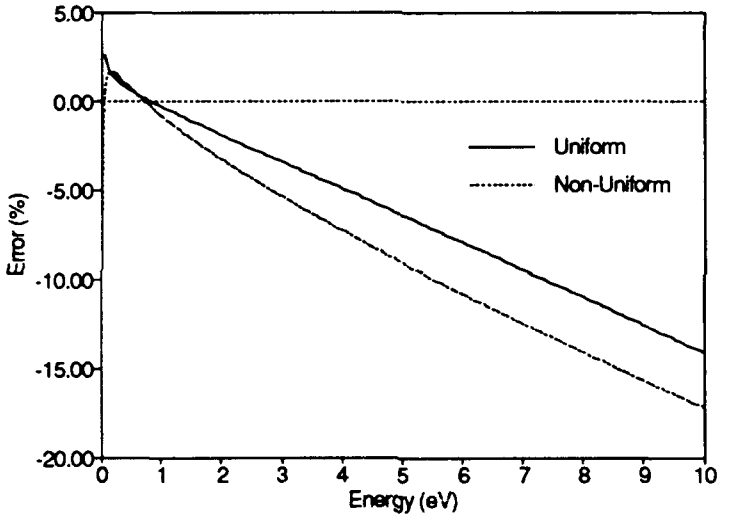

Figure 4. Error in Numerical Calculation: Uniform vs Non-Uniform

The finite differenced term for the momentum transfer recoil was tested for convergence to the proper functional form. In order to do this, the electric field was zeroed, and the momentum transfer collision frequency was held constant at the same value as that which was used previously. The maximum energy of the calculation was varied for each gas temperature such that the distribution underwent at least a six, and not more that a ten order of magnitude drop between

the lowest and highest energies. The number of energy bins along the energy axis was held constant at 200. With no external forces applied to the system of electrons, the distribution should relax to a Maxwellian whose average energy is 3/2 the gas temperature. Table 3 illustrates the results for a variable mesh grid.

Table 3

<E> (eV): 0 Electric Field, $\nu_{M.T.}$ = Const, Calculated for Non-Uniform Energy Grid

Gas Temp (K)	Analytic	Calculated	% Error
300	3.876E-2	3.819E-2	1.471
600	7.752E-2	7.780E-2	0.361
900	1.163E-1	1.168E-1	0.430
1200	1.550E-1	1.560E-1	0.645
1500	1.938E-1	1.948E-1	0.516

Figure 5 shows the converged solution plotted as a reduced distribution for a T_{gas} of 300 K. In this case, α was 0.0005 and Emin was 0.01 (Eq (63)).

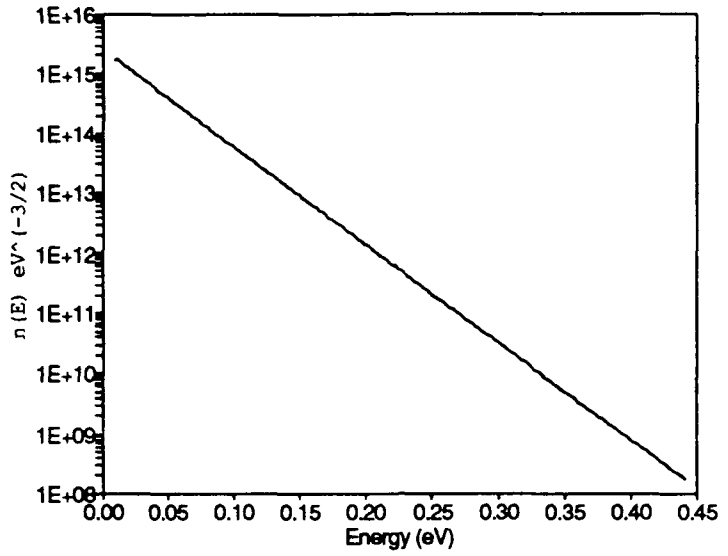

Figure 5. EDF Calculated on Non-Uniform Energy Grid for T_{gas} = 300 K, E/N = 0

Transport Parameters for Gases

Electron EDF's were calculated for Ar and H_2 using both a variable and uniform energy grid. The resulting transport parameters were calculated in each case and compared to experimental data as reported by Dutton (5). In the case of Ar, the parameters were drift velocity, average energy, and α/N. The processes considered for the Ar calculations were momentum transfer, ground state ionization, and three excited states, each from the ground state. The cross sections for these processes are shown in Figure 6.

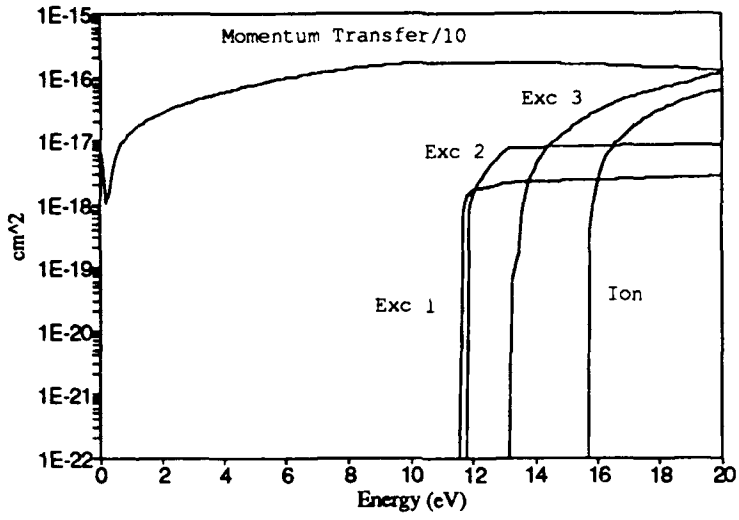

Figure 6. Argon Cross Sections

Figure 7 compares the drift velocities to data gathered by Dutton (5). Although there is significant scatter in the data, the calculated velocities follow the general trends in the data. The data against which the calculated velocities are compared was measured by five different researchers, with two of them causing the largest scatter here.

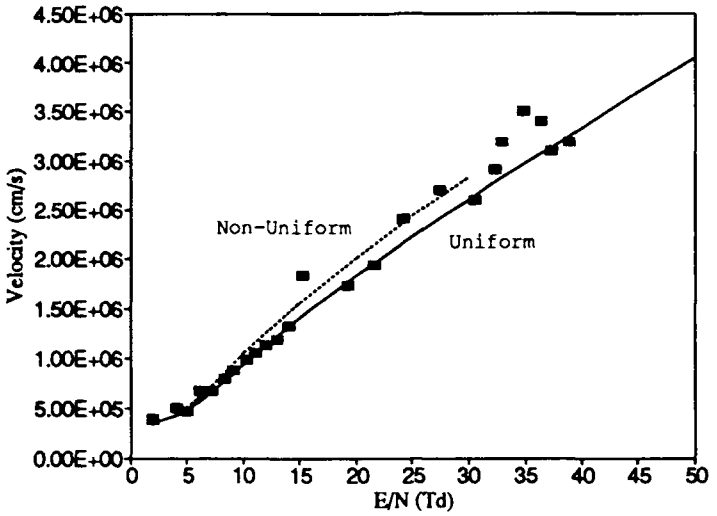

Figure 7. Ar Drift Velocity vs E/N (Data from Ref 5:612)

Figure 8 shows a comparison between the calculated characteristic energy and the data, which was also given as characteristic energy. Again, the general agreement is fairly good. A good agreement between the calculated and experimental values of energy and v_d indicate that the bulk of the electron distribution has been accurately computed. This is due to the characteristic dependence of both these parameters on the bulk of the electrons, or those electrons in the distribution that are below the excitation and ionization threshold energies of the gas.

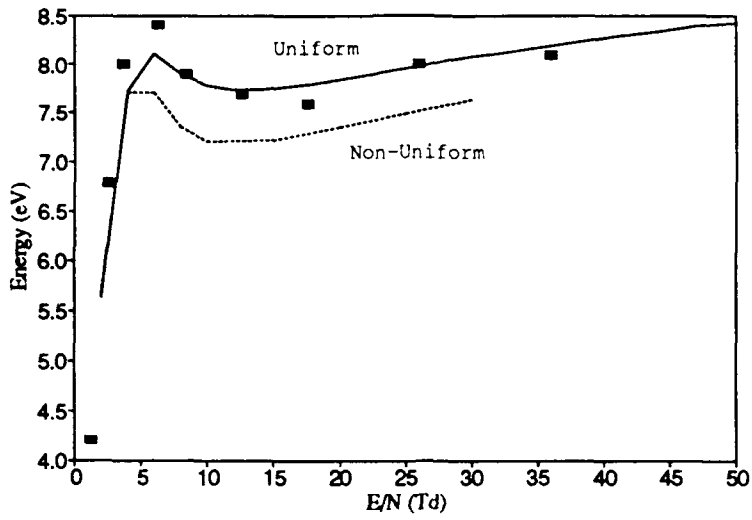

Figure 8. Ar ε_k vs E/N (Data from 5:651)

α/N is a parameter which is characteristic of the tail of the electron distribution. Thus, if the calculated α/N follows the experimentally determined values, then confidence in that part of the distribution governed by the ionization process is established. Figure 9 shows the calculated values of α/N and the experimental data. The calculated values were computed without any superelastic process, thus the slight under-estimation could be corrected by assuming some excited state population ratio in the computation. This would allow the superelastic processes to drive electrons out to the higher energies, thus increasing the ionization rate and thereby the α/N. This under-estimation is also compounded by the numeric ionization rate calculation method, which in the code is a simple box integrator that steps backward. This backward stepping would underestimate the integration of the distribution with the cross section, thus under-estimating the ionization rate, and therefore the α/N. This effect is especially prominent if the distribution falls off rapidly with energy.

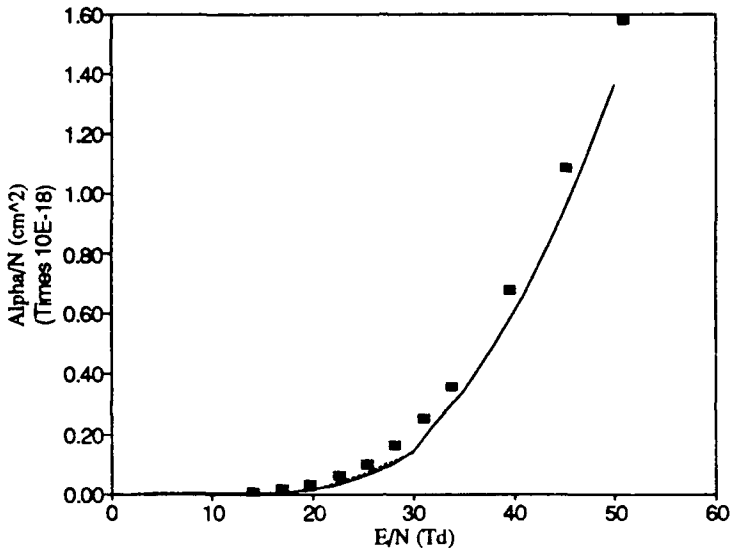

Figure 9. Ar α/N vs E/N (Data from 5:724)

The transport parameters calculated in H_2 were drift velocity and ε_k. Figures 10 and 11 show the cross sections used in the calculation of the transport parameters for molecular Hydrogen. Figure 10 illustrates the momentum transfer, and ground state electronic and ionization cross sections. Figure 11 shows the five ground state vibrational processes. No superelastic processes were used. The threshold energies for the inelastic processes in this molecular gas are in sharp contrast to those in the rare gases, such as Ar or He.

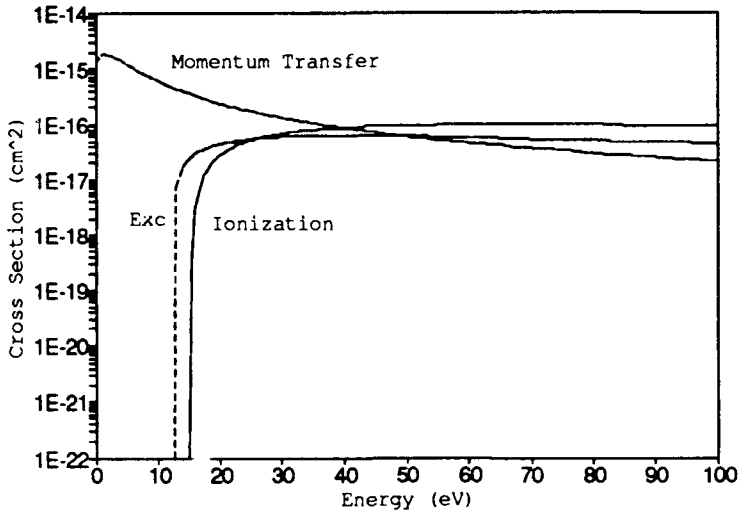

Figure 10. H_2 Cross Sections for M.T., Excitation, Ionization

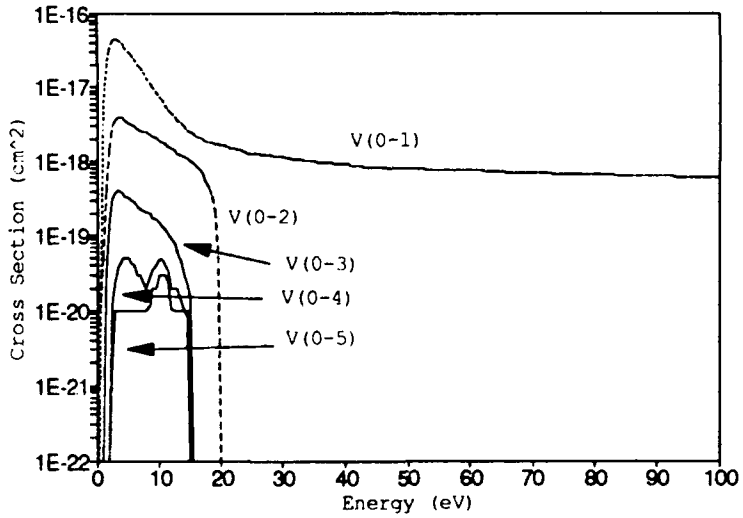

Figure 11. H_2 Cross Sections for Ground State Vibrational Excitation

The drift velocities shown in Figure 12 follow the experimental data fairly well until approximately 30 Td, beyond which the calculated values are greater than the experimental. The velocities computed with the uniform and non-uniform energy grids are in close agreement throughout the E/N range investigated, indicating that this error does not lie in the choice of energy grids used.

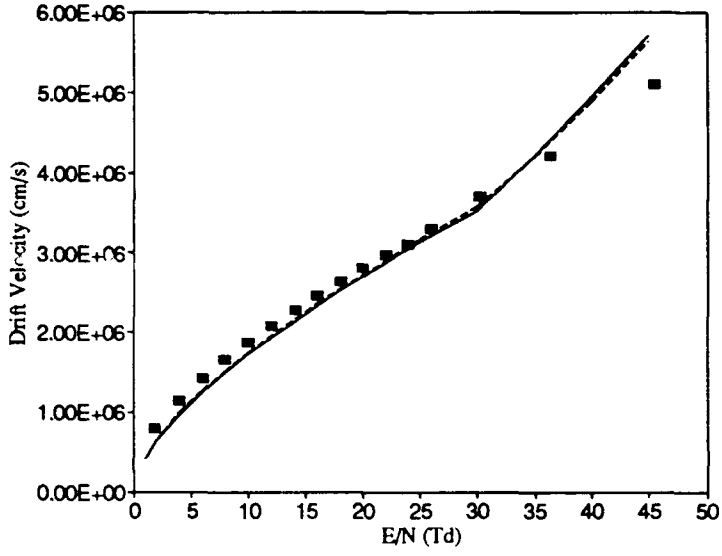

Figure 12. H_2 Drift Velocity vs E/N (Data from 5:618)

The characteristic energy is plotted in Figure 13. In this plot, the calculated average energy has been multiplied by 2/3 in order to obtain an equal weighting with the data, which is given as characteristic energy.

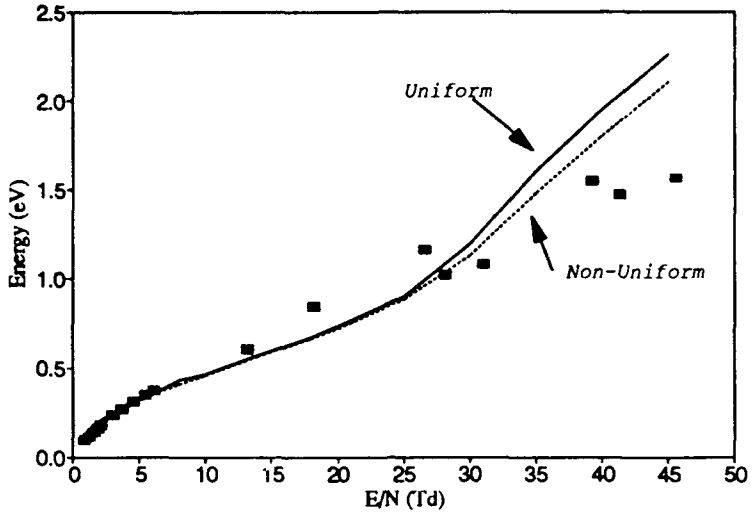

Figure 13. H_2 ε_k vs E/N (Data from 5:655)

In comparing the transport parameters computed with the uniform and variable energy grids for H_2 and Argon, it appears that the computed data for the molecular gas is in better agreement with the data than the rare gas. The calculated parameters for the rare gas generally diverges much sooner. This result is probably due to the higher inelastic thresholds in Argon, at which point the logarithmic grid is becoming excessively large in accurately calculating the distribution.

Validation of Attachment Process

The process of electron attachment was validated by considering the effect that the process would have on the electron distribution, as well as verifying the predictions made by Eq (27) for several special cases. In every calculation, energy balance was considered to be the prime com-

putational diagnostic, with the energy always balancing to within 0.1%. In this validation, the calculations were made on a uniform energy grid of 150 bins, with a maximum energy of 20 eV. Argon was used as the host gas, wherein an attaching cross section was added of varying magnitude and energy dependence, depending on the case. The same E/N value was used for each calculation. The other processes considered were momentum transfer, excitation, and ionization. Figure 14 shows the reduced distribution resulting from the inclusion of an attachment cross section compared to the no-attachment case. For this case, the attachment cross section was constructed such that the attachment rate was constant, given as $\nu_{attach} = 4.0 \times 10^{-11} cm^3 s^{-1}$. The rate was defined as $\nu_{attach} = \sigma(\varepsilon)\nu(\varepsilon)$ $[cm^3 s^{-1}]$ at each energy. With a constant attachment frequency, the rate at which electrons will be removed from each energy bin will be constant, thus the distribution will assume the same form as if attachment were not considered. In as much as the total electron number density is smaller in the case in which attachment is considered, a similar form translates into $n_1/n_2 = \text{constant}$. As expected, the form of the distribution remains similar, although the distribution in which attachment was considered is several orders of magnitude lower than for the case of no attachment. The calculated average energy was the same in each case (3.285 eV), as Eq (27) suggests.

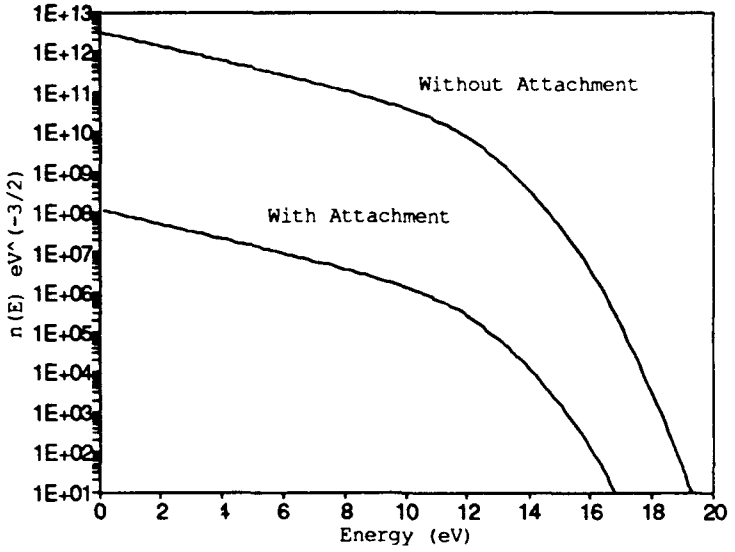

Figure 14. Calculated EDF with a Constant Attachment Rate

Next, an attaching cross section was included such that the rate of attachment increased with energy. The actual rate used rose linearly from 0.0 at 5 eV to $2.0 \times 10^{-8} cm^3 s^{-1}$ at 20 eV. This rate was given as $\nu_{attach} = 1.0 \times 10^{-9} \varepsilon \quad for \varepsilon > 5 \quad eV \quad [cm^3 s^{-1}]$.

This cross section results in electrons at the higher energies having a greater probability of being attached, and as Figure 15 shows, these are the electrons which have been preferentially removed from the distribution. The average energy for this distribution was calculated to be 1.792 eV, clearly indicating the loss of the higher energy electrons.

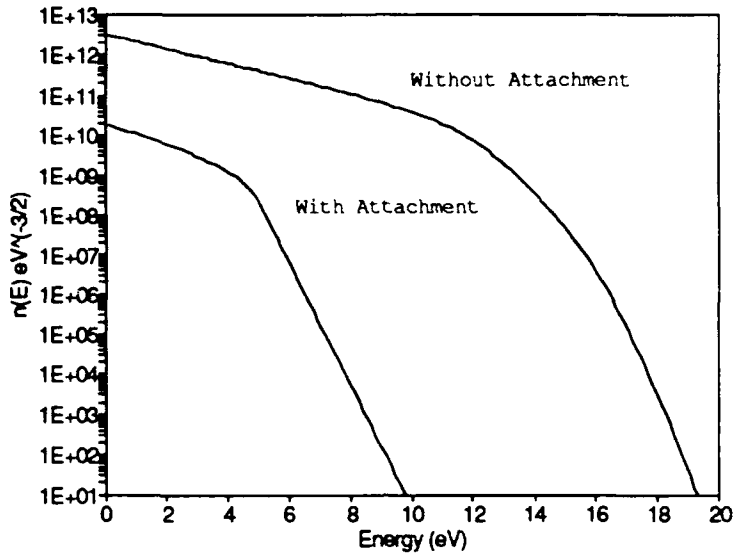

Figure 15. Calculated EDF with an Attachment Rate Increasing with Energy

Finally, an attaching cross section that decreased rapidly with energy was used. This cross section resulted in an attaching rate that also decreased with energy, from a maximum of 4.0×10^{-11} cm^3s^{-1} at 0.01 eV to 0.0 at 2 eV. The EDF with and without attachment are shown in Figure 16. The loss of electrons at the low energies is readily apparent, and in fact, this portion of the curve would have a negative temperature associated with it. This form of the attaching rate will shift the bulk of the electrons to higher energies, resulting in an average energy (5.134 eV) that is greater than that calculated without attachment (3.285 eV).

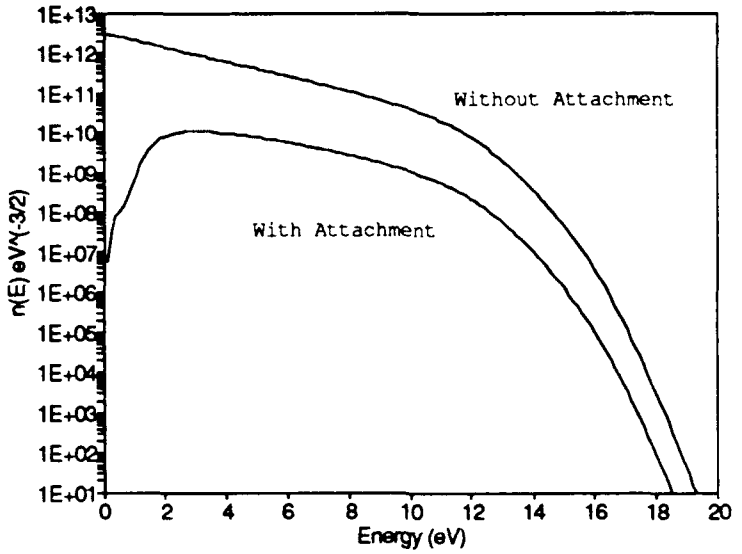

Figure 16. Calculated EDF with an Attachment Rate Decreasing with Energy

Methods of Allocating Variable Energy Grids

Once the code has been validated with the use of a non-uniform energy grid, the natural question that arises is "what is the best grid to use?". A logarithmically allocated bin size is perhaps not the best choice for Argon, a rare gas with little energy separation between the inelastic processes. This is evidenced by the disparity between the transport parameters calculated with uniform and non-uniform energy axes. However, the use of the log grid with H_2 appears to be practical and results in transport calculations that are similar to those calculated with the uniform grid. It would be advantageous if some method could be devised in which the non-uniform energy axis is defined so it would increase the accuracy of the calculation of certain parameters over those calculated with a uniform grid, for the same number of grid points. These parameters

could include normalization of the distribution, drift velocity, average energy, and kinetic rate calculation. The first three of these parameters depends predominately on the bulk of the distribution, while the last depends mostly on the tail of the distribution. Thus, while a non-uniform grid that concentrates bins in the bulk may increase the accuracy of the drift velocity, average energy, and normalization integrals over those calculated with a uniform grid, the resulting kinetic rate information may be much worse than the uniform calculation. Likewise, a grid which places many bins in the tail of the distribution may result in a rate calculation that is an improvement over the uniform grid, but now the other three parameters are far off the mark. The ideal case would be a grid allocated such that the accuracy of all parameters is improved. This is the motivation for Eq (42), with an intelligent choice for the function G.

In order to help explore this possibility, Eq (44) was used as a distribution function. The simplifying assumption that f_o doesn't change much over the interval ε to $\varepsilon + \delta\varepsilon_h$ allows the imbedded f_o terms on the right hand side of Eq (44) to cancel one another. This assumption, while not strictly valid for regions around the threshold energy, will nevertheless allow Eq (44) to serve as a starting point in the dynamic mesh allocation method. With the previous assumption, Eq (44) reduces to a more tractable Eq (65).

$$f_o(\varepsilon) = \exp[-\frac{3}{(E/N)^2}(\frac{2m}{M}\int_o^{\varepsilon} xQ_m(x)Q_r(x)dx + \int_0^{\varepsilon}\frac{Q_i(x)}{x}\int_{\varepsilon}^{\varepsilon+\delta\varepsilon_h} Q_h(y)ydydx)] \quad (65)$$

where f_o is the reduced distribution. Q_h will be assumed to be a step function, with some threshold energy ε_{thresh}, below which the cross section is zero, and above which the cross section is con-

stant. The right hand side of Eq (65) is then analytic, and can be used to represent the approximate solution to the Boltzmann equation, with which the validating parameters are calculated.

$$f_o(\varepsilon) = \exp[-\frac{3}{(E/N)^2}(\frac{2m}{M}\int_o^{\varepsilon} xQ_m(x)Q_r(x)dx$$

$$+\int_0^{\varepsilon}\frac{Q_i(x)}{x}\int_{\varepsilon}^{\varepsilon+\delta\varepsilon_k} Q_k(y)ydydx)] \qquad (66)$$

The parameters used were normalization of the distribution, average energy, drift velocity and excitation rate. Although the distribution function itself was analytic, the integrations required for these comparison parameters could not be carried out analytically when a non-zero inelastic cross section was included in Eq (65). Therefore, these integrations were accomplished numerically, using a uniform energy grid of 400 points, and used as the "standard". The other uniform and non-uniform integrations were made on a 50 point grid, and compared to this standard.

Several choices for the function G in Eq (42) were tried, with varying degrees of success in improving the calculation of the normalization, drift velocity, and kinetic rate over the uniform integration. The choices for these merit functions were driven by their respective influence on the placement of energy bins on the dynamic energy axis. Since an allocation function which would place more bins in the body of the distribution wouldn't aid in the rate calculation, and vice-versa, two merit functions were used to work in conjunction with each other. In this method, the final merit function was the average of two others, one designed to aid the calculation of bulk dependent parameters (average energy, drift velocity) and the other designed to aid in the tail dependent ones (kinetic rates). The function chosen for the bulk optimization was an energy moment of the distribution, where G was represented by

$$G_1(\varepsilon) = \varepsilon^n \varepsilon^{1/2} f_o(\varepsilon) \tag{67}$$

where n is some power. If n = 0, then G_1 would be a normalization integrand. If n = 1, G_1 would be an average energy integrand. Increasing the power of n will shift the peak of G_1 out to higher energies, which will delay the peak of the cumulative integral function F. In testing this algorithm, it was found that the value of n that would result in the best integration of the average energy and drift velocity for the non-uniform grid was dependent on the E/N ratio.

The integration of the tail was aided by constructing a function G given by the rate integrand:

$$G_2(\varepsilon) = Q(\varepsilon)\varepsilon f_o(\varepsilon) \tag{68}$$

Thus $G = G_1 + G_2$.

In integrating the rate parameter, it became apparent that the exact placement of the threshold energy was a very critical variable. Consider a uniform energy grid where the threshold energy is just slightly less than the bin energy, as in Figure 17. In this instance, the bin energy is defined as that energy corresponding to the right hand side of a particular finite differenced bin. If the inelastic cross section rises steeply, and the distribution is falling off rapidly, then the resulting rate integrand will appear as that shown. The simple Simpson backward integrator would result in a large over-estimation of the integral from the first bin containing a non-zero value for the rate. On the other hand, the backward integration of the other bins would always result in the under-estimation of the actual value of the integral. The result of these two effects is that the calculated integral may be high, low, or very close to the actual value of the integral. If the over-estimation is approximately the same as the under-estimation, then the calculated integration will be close to the correct value. This result will occur in spite of the errors in the integration method.

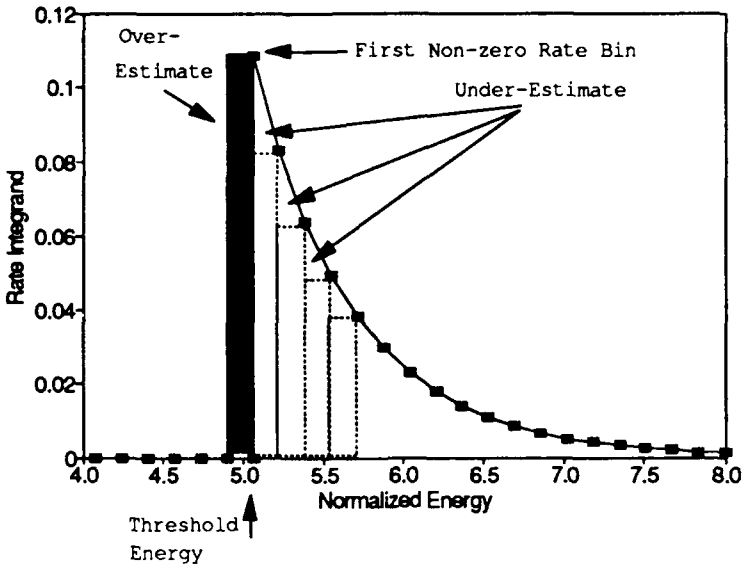

Figure 17. Rate integrand with ε_{thresh} slightly less than a bin energy

Consider now a threshold energy slightly greater than a bin energy, as in Figure 18. In this case, the rate integral is only under-estimated, and could be worse than the value calculated by the previous method.

With the non-uniform energy grid construction technique used here, the bin before the threshold energy is typically fairly wide, resulting in a significant over-estimation of the rate integral. This is especially so with the addition of many more bins into the region due to the more accurate integration in the following bins. Therefore, the placement of a bin at the threshold energy becomes an important step in accurate rate calculation.

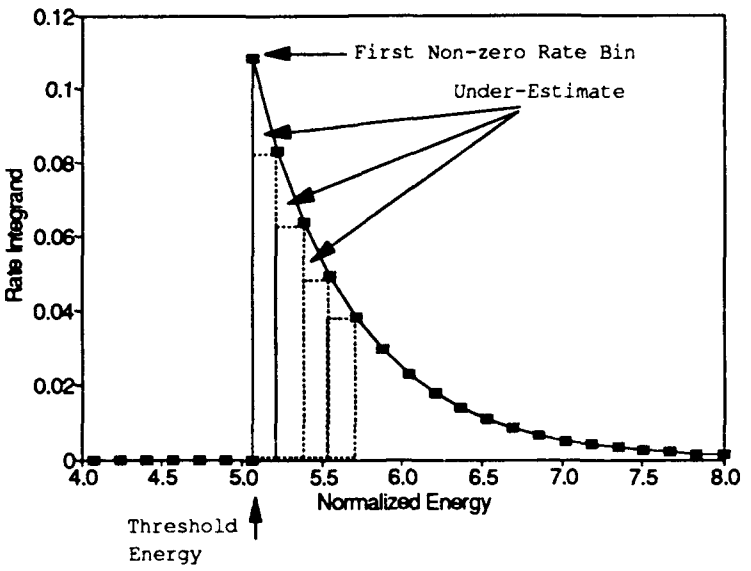

Figure 18. Rate integrand with ε_{thresh} slightly greater than a bin energy on uniform energy grid

Figure 19 shows the result of using this choice for an energy bin allocation function in defining a 50 point non-uniform grid. In this plot, the normalized distribution function and normalized rate integrand are shown in order to visualize not only the construction of the allocation function itself, but also in order to understand the resulting integrations of each over the variable energy axis, which is shown as the variable size grid. The inelastic threshold is at an energy of 5.06.

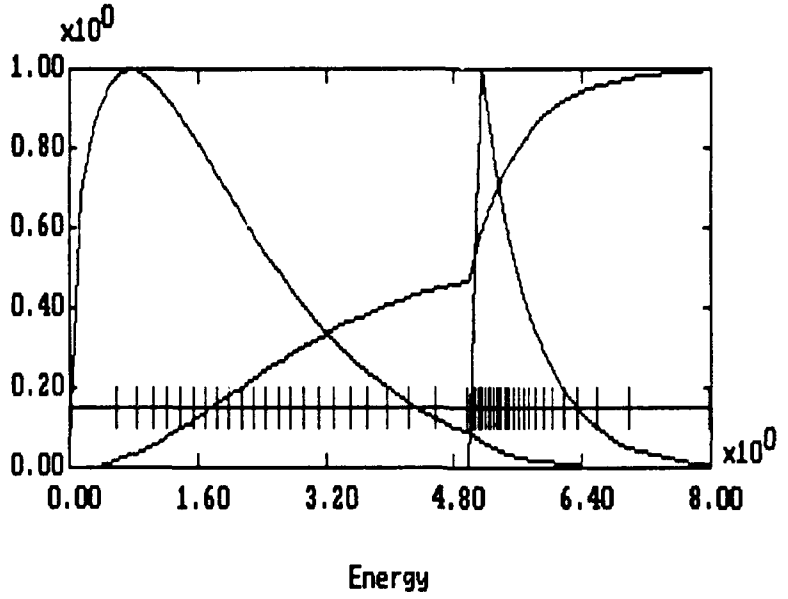

Figure 19. EDF and Rate Integrand and resulting Allocation Function

It is instructive to see how the variable energy grid will integrate each of the parameters of interest. Figure 20 shows each of these parameters in a box layout. At the top left is shown the energy moment of the distribution along with the energy grid resulting from the merit function of G. The integral of this function yields the average energy. Below the energy moment is the rate integrand. The increase of the bin density in this region always resulted in a more accurate rate calculation compared to the uniform method. The top right panel illustrates how the variable axis will integrate the anisotropic part of the distribution, which yields the drift velocity. The bottom right plot shows the symmetric part of the distribution function, whose integration will result in the normalization that is used in both the rate and drift velocity calculations.

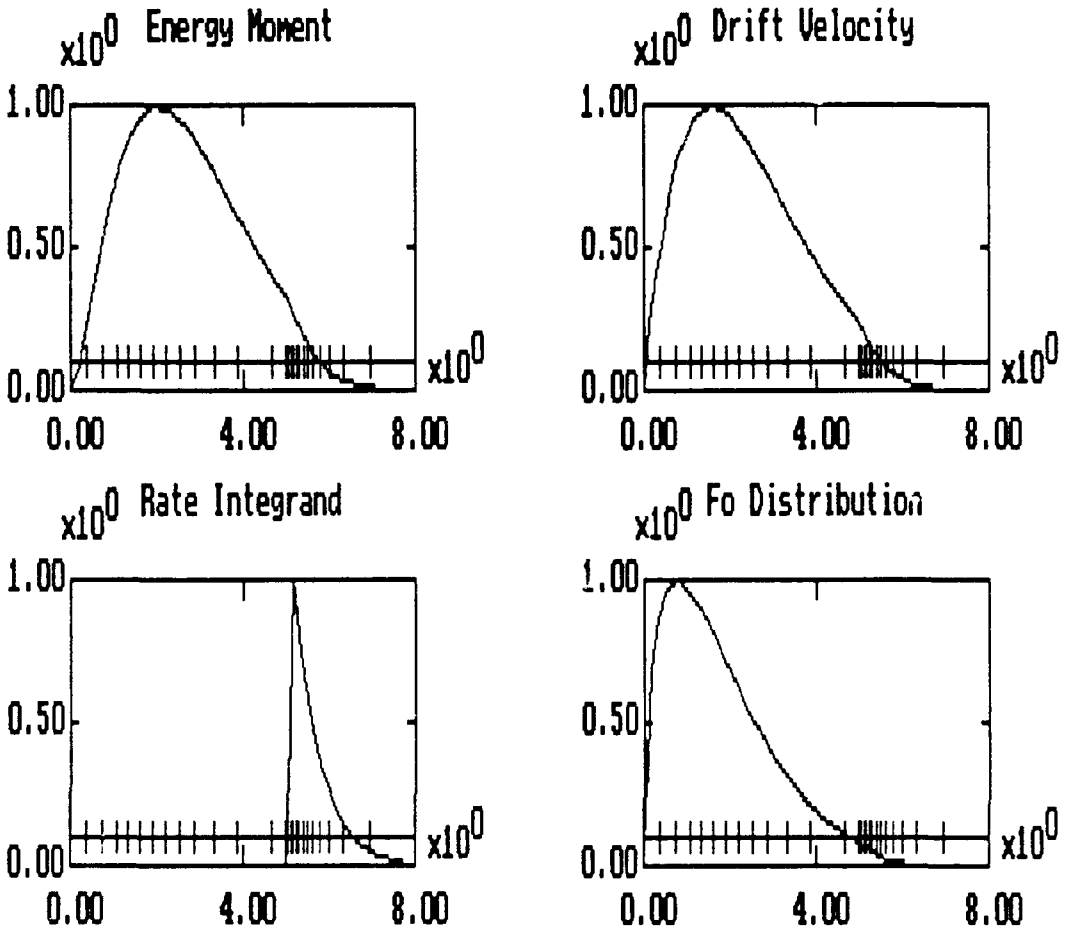

Figure 20. Non-Uniform Energy Grid with Validation Parameters

Figure 21 shows the allocation function G, where n = 1.0 in Eq (66), at 5 Td and the distribution and rate functions from which it is constructed. Comparing this plot to Figure 22, which is for the same conditions except n = 0.2, leads to some interesting points. As the value of n increases, its effect on the allocation function is evident where the slope is reduced at the lower energies, resulting in a less dense allocation of energy bins in this region. Varying the value of n has little effect on the allocation of energy bins at the higher energies where the inelastic cross section lies, thus the calculation of the rate varies little.

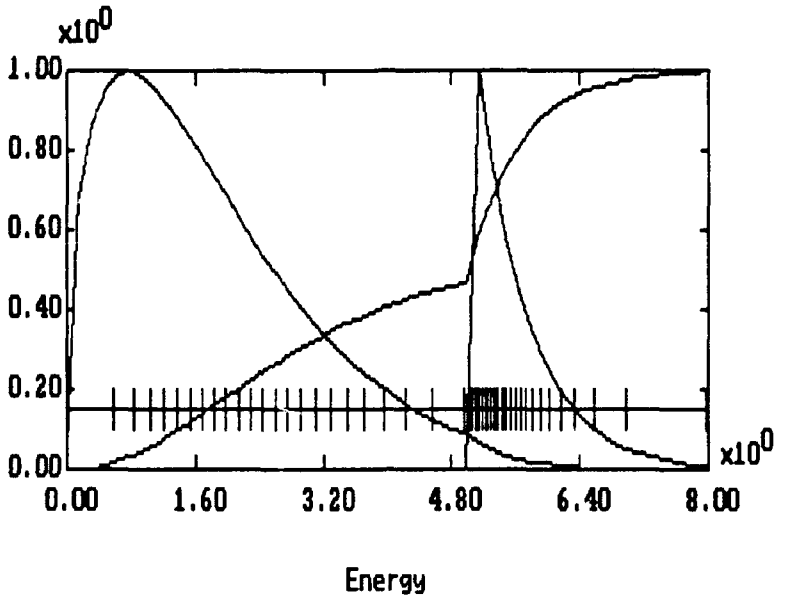

Figure 21. Allocation Function for 5 Td, n = 1.0

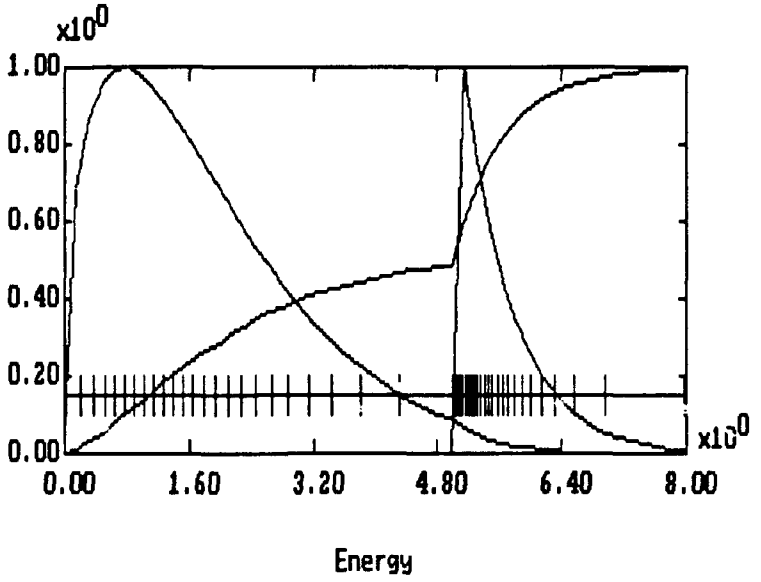

Figure 22. Allocation Function for 5 Td, n = 0.2

Figure 23 shows a comparison of the validation parameters for different values of n, with the uniform calculations for the same number of bins. It was found that the optimum value of n in Eq (66) for 5 Td was 0.6. At n values lower than 0.6, the calculated normalization, average energy and drift velocity parameters were all under-estimating the standard, while higher values led to an over-estimation. Varying the n value had a very small effect on the non-uniform rate calculation, which was always better than the uniform calculation, and is not included in this plot.

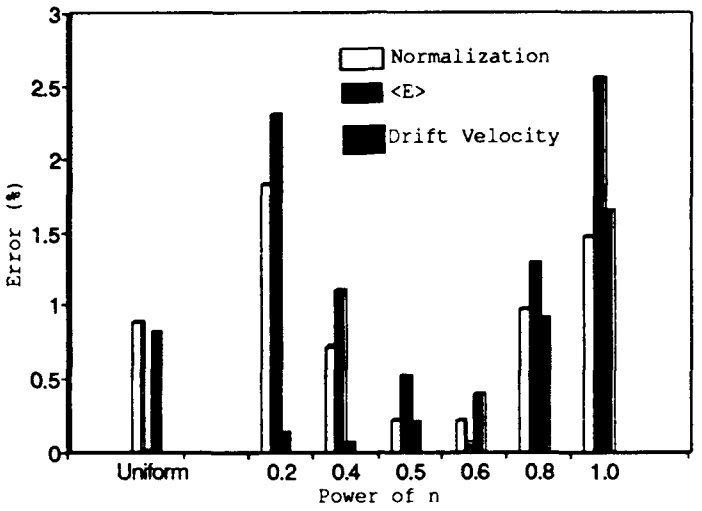

Figure 23. n vs Percent Error for 5 Td

As the E/N ratio is reduced, the distribution becomes more localized toward the lower energies, which results in the optimum n value increasing, as seen in Figure 24. Figures 25 and 26 illustrate how the different n values lead to their respective integrations of the validation parameters. At the higher n value (Figure 25) the smaller slope of the allocation function at low energies allows more bins to placed in the region where the distribution is falling off rapidly. Although this movement of energy bins to the higher energies results in a poorer integration of the low energy portion of the distribution, it is offset by the increased accuracy at the higher energies. The lower n value (Figure 26) leads to too many points allocated near the origin, thus under-estimating the integration of the tail.

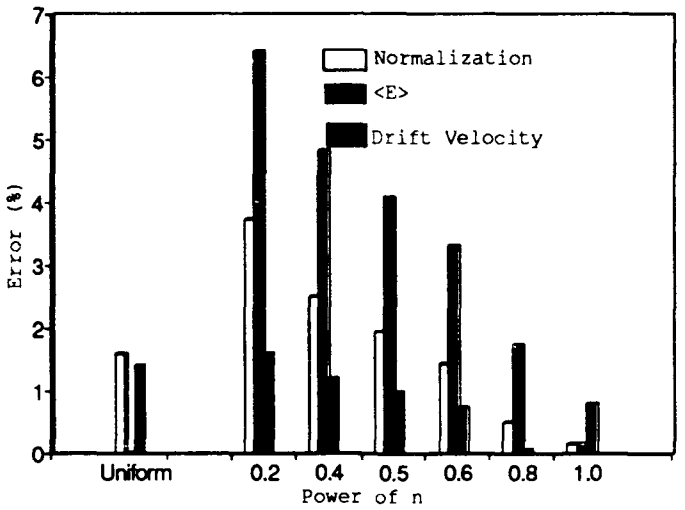

Figure 24. n vs Percent Error for 4 Td

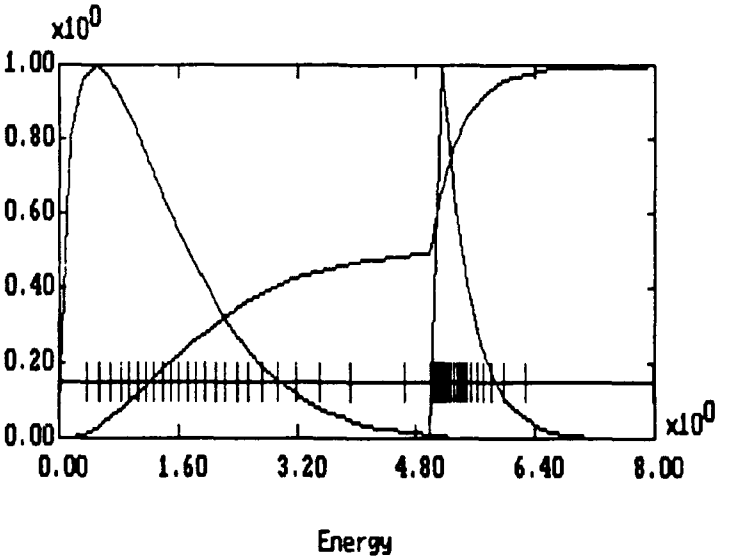

Figure 25. Allocation Function for 4 Td, n = 1.0

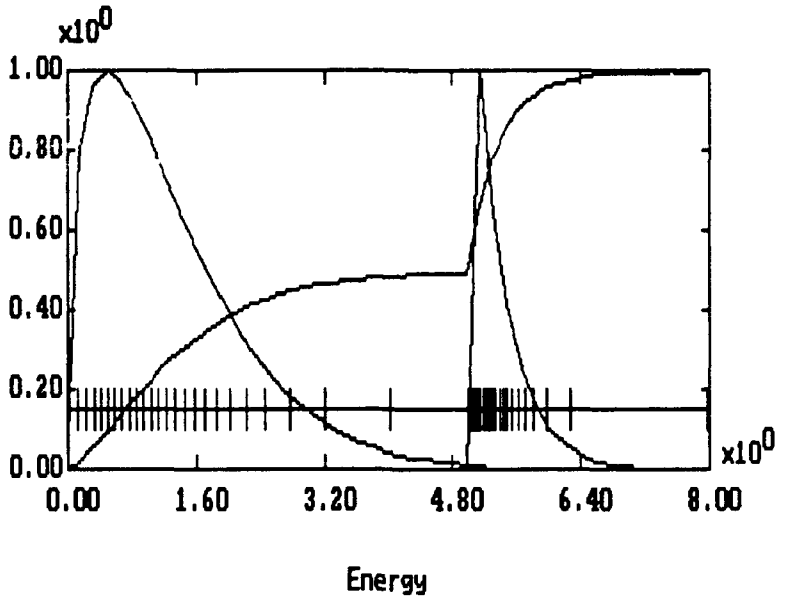

Figure 26. Allocation Function for 4 Td, n = 0.2

It is interesting to note that even with the optimum value of n used for the non-uniform calculations, a 3.8% increase in the accuracy of the rate comes at the price of a 38.8% increase in the number of bins in the cross section region.

Electron-Electron Collisions with Non-Uniform Energy Grid

It is well known that electron-electron collisions tend to Maxwellianize the distribution, thus smoothing out any sharp features that tend to result from inelastic collisions. In the absence of any other effects, electrons colliding with themselves will relax toward a Maxwellian with an electron temperature equal to 2/3 of the average energy. The electrons must obey this property regardless of the initial distribution. Conservation of energy and of particles must also be obeyed with each iteration.

The electron-electron interactions on the non-uniform energy grid were tested in several

ways. With an initial distribution of a Maxwellian with a temperature of 2/3 the average energy, the iterative solution was allowed to propagate forward in time. The test for the distribution convergence was disabled, allowing each time iteration to proceed until a fixed number of loops through the electron collision subroutine were accomplished, in this case 2000. Figure 27 shows the resulting distribution, along with the initial Maxwellian distribution.

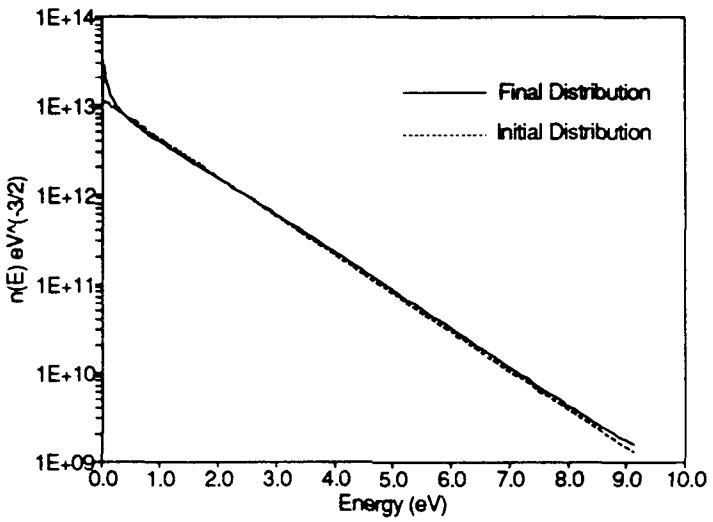

Figure 27. EDF with electron-electron collisions only

The initial distribution was observed to depart from the Maxwellian as the program iterated through the solutions. This departure is more evident at the lower energies. Conservation of energy and of particles were obeyed at each iteration, within the limits of the numerical representation of each. When this test case was performed on the uniform grid, the initial and final distribution were exactly the same out to at least six decimal places, with conservation of energy and particles observed. The deviation from the Maxwellian with the algorithm using a non-uniform

grid indicates that the $A_{k,l}$ matrix is not properly constructed. Since the particles are conserved, the boundary conditions applied to this matrix seem to be correct. The relationship between the $A_{k,l}$ and $B_{k,l}$ matrices also appears to be correct due to energy conservation.

In order to test the algorithm's ability to relax to the Maxwellian form, an initial distribution was constructed with 3.6×10^{12} electrons at 1.5 eV, and a small fraction (1.0×10^{5}) in every other bin. The temperature of the resultant Maxwellian must then be very close to 1 eV. Figure 28 shows the distribution at various points throughout the iteration sequence. Since the time step used was 0.2 ns, the distributions at 500, 1000, and 1500 iterations correspond to times of 100 ns, 200 ns, and 300 ns respectively.

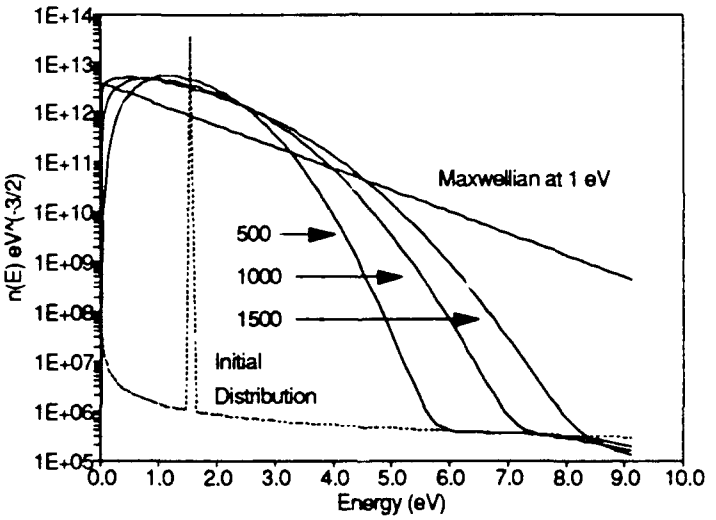

Figure 28. EDF with electron-electron only; spike initial distribution

Although it appears that the distribution is slowly relaxing to the Maxwellian at an electron temperature of 1 eV, conservation of energy and of particles was not obeyed to all orders. The number density of electrons was observed to increase with time, causing the system to therefore gain energy with time. This breakdown indicates a probable error in the implementation of the

boundary conditions, even though conservation of particles was obeyed in the previous test case. Even though the relationship of the $A_{k,l}$'s and $B_{k,l}$'s was designed such that conservation of energy is always obeyed, this cannot hold if the particles are not conserved. When this same test case was performed with the uniform grid, conservation of energy and particles was observed at each iteration, with the distribution approaching the 1 eV Maxwellian in approximately the same manner as Figure 28.

Electron Beams

In order to isolate the effect of the electron beam alone, the electric field was turned off, thereby eliminating any field driven flux. A logarithmic energy axis was used, and a point source of electrons was placed at 60.4 eV. The maximum energy of the grid was just slightly greater than this value. A beam current of 10 Amps was introduced into the H_2 gas, which was at 1 atmosphere and 300 K. The processes considered were vibrational excitations from the ground state to levels 1 through 5, the first electronic excitation from the ground state, and ground state ionization. Figure 29 shows the converged solution 26 ns after the beam turned on, with a Maxwellian being the initial distribution. For the electrons being injected into the plasma at 60 eV, there are only two places to go. They can either excite the ground state to the first electronic state (12.6 eV), or they can ionize the ground state H_2 molecule (15.427 eV). The large increase in population at 47 eV is due to the first process, while the peak at 44.5 eV is due to the second.

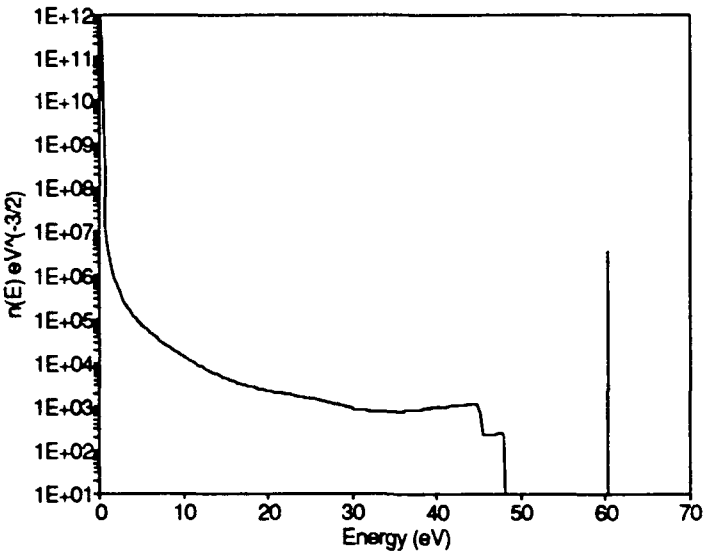

Figure 29. H_2 EDF with Electron Beam Source at 60.4 eV

In the calculation of this distribution function, it was necessary to zero all momentum transfer flux out of the energy bin containing the source beam. Without doing so resulted in a distribution centered around the source that was widely spaced in energy, covering approximately 25 eV. This broad region was due to the large downflux of electrons due to recoil with the heavy particles. Additionally, in the region between the secondary peaks and the source it was necessary to set a lower limit on the number density of electrons in the energy bins. Due to the constant depletion of electrons in this region without any influx of electrons from either below or above, the population will continue to decrease with each iteration of the time-dependent solution. As a result, the computation went unstable (ie, negative number densities) when the computer reached its smallest representable number, which was of the order of 10^{-300}. In order to avoid this from happening, an articial lower limit of 1×10^{-50} was placed on the electron densities at these energies.

The distribution is relatively flat across the intermediate region due to the small energy coupling between the H_2 molecules and the electrons, which is $2m/M$. In this region momentum transfer is the dominate energy transfer mechanism. The electrons will continue to exchange energy with the heavy particles in this manner until the vibrational cross sections become effective. At the very low energies (approximately 2 eV and below), the gas molecules at 300 K are again exchanging energy with the electrons, with the distribution becoming a Maxwellian at appromimately this same temperature.

In comparing this distribution to that calculated by Bretagne (3:821), the same general features are observed. However, there is much more structure in Bretagne's calculation of the distribution. It appears that the first spike in the his distribution below the source beam (50 eV) is due to electronic excitation in H_2, either 1s to 2p or 1s to 2s, both of which have a 10.2 eV threshold. The large population just below this (45 eV or so) is probably due to ionization. The gap that appears between these two peaks is likely explained by Bretagne's consideration of electron loss mechanisms, specifically recombination and diffusive wall losses. These effects were not considered in the present calculation, and the resultant lack of structure between the two peaks in Figure 29 is due to a large momentum transfer downflux from the energy bin filled by electronic excitation. Likewise, any structure that may appear in the intermediate region is "washed" smoothly away due to this same effect. By introducing loss mechanisms, not all of the electrons will be able to collide elastically with there collision partners, since many will be lost out of the continuum due to the recombination or diffustion. As a result, the downflux of momentum transfer from one energy bin to the next lower bin will be reduced, and the structure that Bretagne reports may then be observable.

The calculated solution with the source at 90.0 eV is shown in Figure 30. The basic structure of the distribution is similar to that with the 60.4 eV source. Here again, the differences between Bretagne and the calculated distribution lie in the lack of detailed structure.

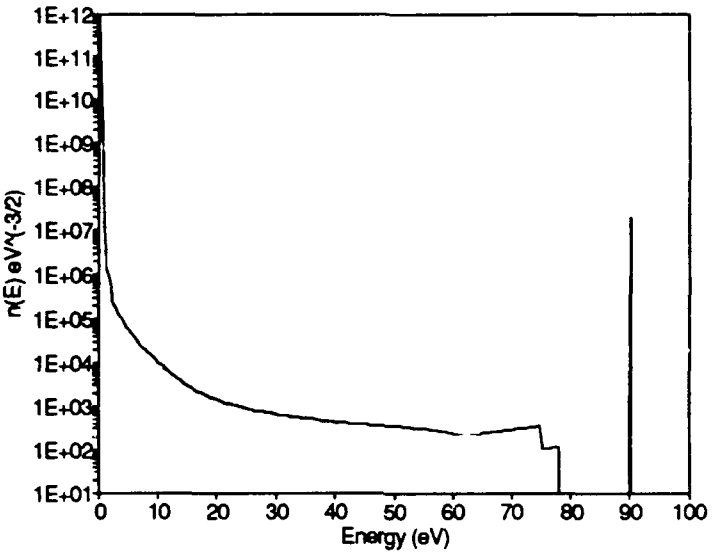

Figure 30. H_2 EDF with Electron Beam Source at 90.0 eV

Negative Total Electron Mobility

In order to explore the possibility of negative mobility, the solution method utilizing the time-dependent Boltzmann equation was exercised under various conditions of physical interest. Since the principle means by which a negative mobility, and therefore a negative drift velocity, can occur is a low energy loss of electrons, this process in the form of attachment was included. Fluorine, which has a large attachment cross section at low energies, was used as the attaching gas, with Argon used as the primary gas. Several gas concentration levels were explored, resulting in a strong influence on the drift velocity.

The momentum transfer and attachment cross section for Fluorine are shown in Figure 31. The large cross section for attachment at the low energies results in a high probability of the

electrons to be lost at these same energies. Since the cross section falls off very rapidly, the electrons at energies greater than 2 eV or so will be largely unaffected, with the result being a reduced distribution with a positive slope at low energy, and a more traditional negative slope at the higher energies.

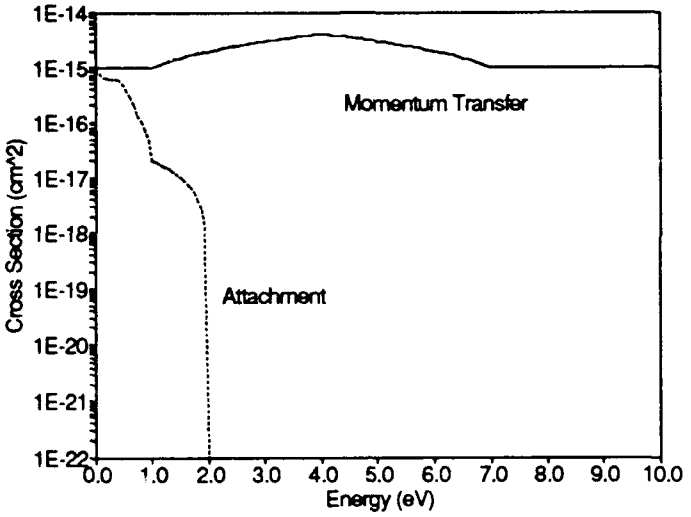

Figure 31. Fluorine Cross sections

The energy distribution calculations were performed on a 150 point uniform energy grid, that was typically 8 eV at the maximum energy. Initially, a gas mix of 100% Ar and 0% F_2 was used to validate the drift velocities calculated from the code. The calculated drift velocities were compared with data (5:612) resulting in fair agreement (Figure 32).

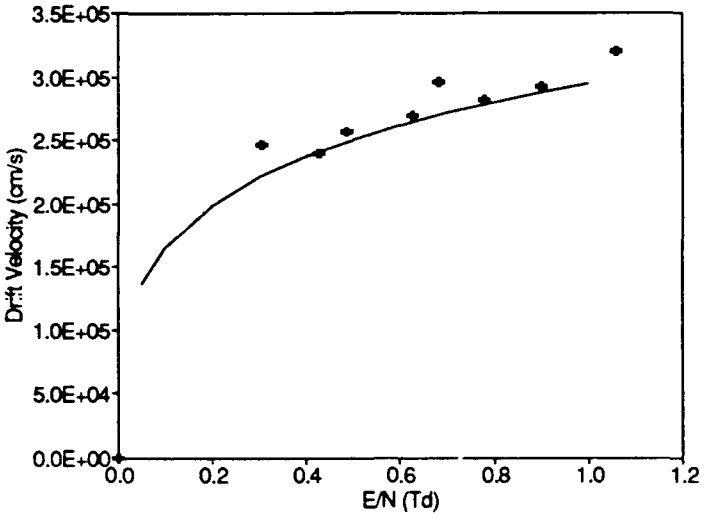

Figure 32. Drift Velocity in Argon at Low E/N

Two mixes of Ar/F_2 were used, the first being 99.9% Ar with 0.1% F_2, and the second 99.5% Ar and 0.5% F_2. At low E/N, the field driven flux is very weak, resulting in a distribution that falls off rapidly at higher energies. This rapid decrease in the distribution is due to the small field driven flux combined with the Argon momentum transfer cross section that increases rapidly with energy, resulting in a collision frequency that increases rapidly. As this collision frequency increases, the elastic energy transfer becomes greater, resulting in the steep negative slope. At the low energies, the attachment process will continually serve as an electron sink, resulting in a distribution with low populations in this energy region. The EDF for a 99.5/0.5 mix of Ar/F_2 at 0.5 Td is shown in Figure 33. The low energy region with the positive slope is responsible for the negative drift velocity. This region also has a characteristic temperature that is negative.

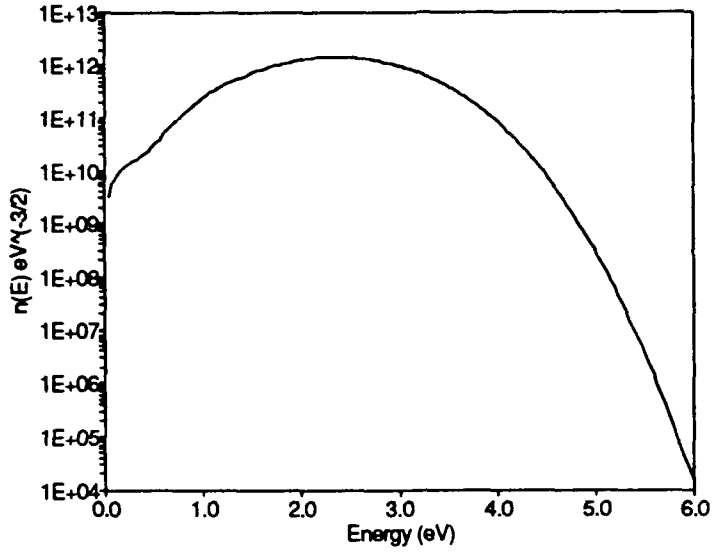

Figure 33. EDF in Ar/F_2 for 99.5%/0.5% Mix at 0.5 Td

The resulting drift velocities are plotted against E/N in Figure 34. The distribution with the higher concentration of Fluorine requires a greater upflux of electrons in order to recover a positive drift velocity. Since this upflux is caused by the electric field, a larger E/N ratio is required to obtain a positive drift velocity compared to the lower concentration case.

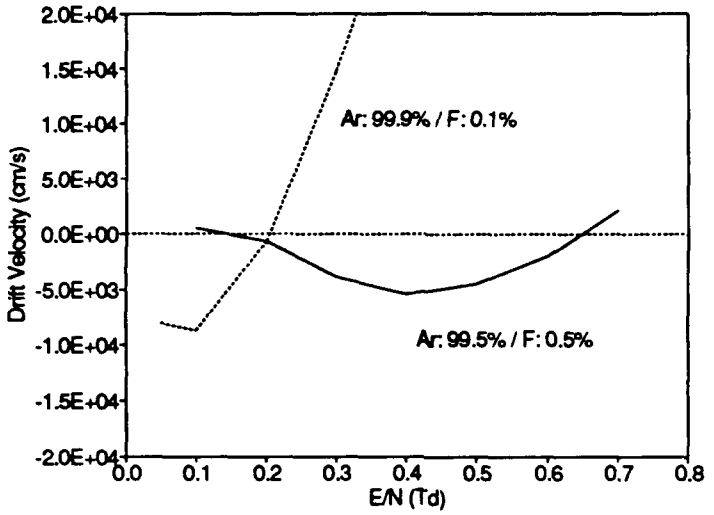

Figure 34. Drift Velocity in Ar/F_2 vs E/N

In both mixtures, as the E/N is increased, the field driven flux increases, while the effect of the attachment process is reduced. This results in the calculated drift velocities for both mixes approaching that of pure Argon, with the lower F concentration case approaching it much sooner.

VI. Conclusion and Recommendations

The code developed by Seger (16) has been improved to include the processes of superelastics, attachment, and excitation and ionization from excited states. The capability to solve the Boltzmann equation on a non-uniform energy grid has also been added to the code. This added capability is essential in order to extend the energy range of the solution past a previous upper limit of 30 eV or so. With the non-uniform energy grid, the upper limit has been increased threefold, to a demonstrated 90 eV. These larger energy ranges are essential in order to explore the effects of an electron beam on the energy distribution functions, which have been calculated under conditions typical for a hydrogen magnetic multicusp discharge. In addition, the recoil term for momentum transfer has been finite differenced using a new method that recovers the expected Maxwellian form in the absence of electric fields, as well as maintaining numerical stability under this same condition, both of which were lacking in the previous version of the code. Transport parameters computed with the non-uniform energy grid are generally in agreement with those calculated with the uniform grid as well as experimental data. The use of the logarithmic grid yields more accurate computations of the transport parameters for H_2 than for Ar. This is likely due to the grouping of inelastic processes at the lower energies in H_2, whereas in Ar the inelastic processes occur at higher energies. It is expected that the accuracy of the calculation of the transport parameters with a log grid in He would be worse than in Ar, due to its greater inelastic thresholds. The optimization of the construction of a non-uniform grid has been explored with limited success. A more accurate kinetic rate calculation is quite feasible, although it seems that the price for such comes in the form of a less accurate calculation of the drift velocity, average energy, and normalization - parameters which depend mainly on the bulk of the distribution. The benefit of placing an energy bin at the threshold value of each inelastic process is established, resulting in a more accurate kinetic rate calculation. The utility of this "threshold marking" technique is enhanced when a cross section with a large slope at threshold is

used. Finally, the possibility of steady state negative drift velocities has been explored in lean Ar/F_2 mixtures. The numerical calculations indicate that at low E/N values and with the proper gas concentrations, negative drift velocities can be achieved.

While these added capabilities increase the ability to analyze plasmas, more can and must be done to increase the accuracy of the solution, as well as the transport parameters computed from it. A better method for establishing the non-uniform axis is essential in order to achieve its potential at being more accurate than the uniform axis. As shown previously, the logarithmic grid is better in molecular gases than in rare gases, with the uniform axis being generally better in either. However, it is still maintained that with the proper grid the non-uniform can be better than uniform, at least in the calculation of some of the parameters of interest. The optimization of this non-uniform grid needs to be explored more fully in order to achieve this goal.

In electron beam generated plasmas, the inclusion of recombination and diffusive wall losses appears to be important in reproducing the structure that the distributions calculated by Bretagne (3) exhibit. Additionally, electron - electron interactions within the electron beam generated plasma will tend to Maxwellianize the distribution, and thereby serve to smooth out any sharp structure arising in the distribution from inelastic collisions. Therefore, its inclusion into the solution method is important, especially at the higher fractional ionization levels.

Another problem with the present code exists in the finite differenced terms for the field driven flux when used in conjuction with an e- beam. As has been reported, very sharp structure can result in the distribution as a consequence of the electrons being fed at high energies, and relaxing to lower energies through inelastic collisions. The field driven flux term includes a first and second derivative of the electrons number density with respect to energy. Since any sharp features in the distribution will cause both of these derivatives to be discontinuous, numerical instabilities around these regions have resulted when the present code is used with both an electric field and an electron beam. It may be possible to eliminate part or all of this instability by

finite differencing the field driven flux term to higher orders and/or using a central difference scheme in place of a forward difference one. Doing so, however, will result in the C matrix no longer being tridiagonal, which will increase the time required to decompose it.

In order to isolate the electron beam generated plasma from the presence of an electric field, the recoil momentum transfer flux term had to be finite differenced in a new way, based on that used by Greene and Elliott (6). With no electric field, and in the absence of any source, this version of the recoil flux term has maintained numerical stability and reproduced a Maxwellian at a temperature of 2/3 of the average gas temperature as required by physical laws. However, when this representation of the recoil term was used in conjunction with an electric field in Argon, the distribution was overpopulated at the lower energies, and underpopulated at the higher ones. The resultant transport parameters were also well off the experimental values. Returning to Rockwood's recoil term re-derived for the non-uniform energy grid (Appendix A) resulted in the proper calculation of the distribution function and its transport parameters. However, when this version of the recoil term is used in the absence of an electric field, numerical instability is the result. It would seem likely that there is some value of the electric field at which Elliott and Greene's version will produce correct results. More testing and investigation is required in order to determine where the cutoff between one representation and the other will be.

Appendix A

Derivation of field and recoil flux terms for a non-uniform energy axis

Although the terms representing the flux of electrons through energy space due to the applied field and recoil have been derived in the past, the inclusion of a non-uniform energy axis requires that they be rederived explicity. In this section, they will be considered separately, and then grouped together at the end. First, consideration will be given to the field driven flux term, with the momentum transfer term following. The energy axis will be define as

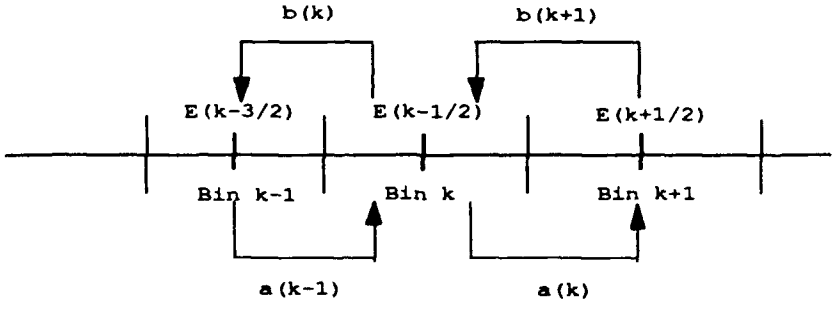

Figure 35. Energy Axis for Momentum Transfer

Field Driven Flux

The origin of the field driven flux term as presently implemented in Megaboltz stems from a paper by Zel'Dovich and Raizer (19), as reported by Greene (7). In this paper, they expressed the continuity of electrons under the influence of an intense electromagnetic pulse as

$$\frac{\partial n(\varepsilon)}{\partial t} = -\frac{\partial J}{\partial \varepsilon} + Q \qquad \text{(A-1)}$$

where J is given by

$$J = n(\varepsilon)u - D\frac{\partial n(\varepsilon)}{\partial \varepsilon}$$

where $n(\varepsilon)$ is the number density of electrons with energy between ε and $\varepsilon + \delta\varepsilon$, u is the "velocity" of the electron along the 1 dimensional energy axis, and D is the diffusion coefficient along the energy axis. The velocity of the electron along the energy axis can be envisioned as being similar to the velocity of the electron through phase space. In such an analogy, the geometric divergence of the flux ($n(v)v$) through phase space is equivalent to the energy divergence of the flux ($n(\varepsilon)u$) through energy space. Here, the velocity of the electron along the energy axis is defined as

$$u = \frac{d\varepsilon}{dt} \qquad \text{(A-2)}$$

The diffusion coefficient in energy space is written analogously to that in geometric space:

$$D = \frac{1}{3}\left(\frac{\Delta\varepsilon}{\Delta t}\right)\Delta\varepsilon \qquad \text{(A-3)}$$

The ratio of $\Delta\varepsilon/\Delta t$ can be expressed as eEv, since the electric field is the only force on the electron in the consideration of the field driven flux. Thus, Eq (A-3) can be expressed as

$$D = \frac{1}{3}(ve\mathrm{E})^2\Delta t \qquad \text{(A-4)}$$

The assumption is made that every time the electron collides with a heavy particle, it will give up all of its excess energy. Doing so allows Δt to be expressed as $1/\nu_m$, where ν_m is the momentum transfer collision frequency. Eq (A-4) can then be written as

$$D = \frac{2(eE)^2\varepsilon}{3\, m\nu_m} \tag{A-5}$$

It will prove to be advantageous to express Eq (A-5) in terms of E/N:

$$D = \frac{2N^2e^2(E/N)^2\varepsilon}{3\quad m\nu_m} \tag{A-6}$$

The "velocity" u can be expressed in terms of the diffusion coefficient as (19):

$$u(\varepsilon) = \frac{D}{2\varepsilon} \tag{A-6}$$

Finally, then, the current density in energy space due to the applied field can be expressed as:

$$J_f = \frac{2}{3}N\frac{e^2(E/N)^2\varepsilon}{m(\nu_m/N)}\left(\frac{n}{2\varepsilon}-\frac{\partial n}{\partial \varepsilon}\right) \tag{A-7}$$

which is Eq (5). So now it becomes necessary to finite difference this equation in energy space. A simple backward difference expression for this differencing will be used:

$$\frac{\partial n}{\partial t} = -\frac{\partial J_f}{\partial \varepsilon} = -\left(\frac{J_f(k)-J_f(k-1)}{\Delta\varepsilon_k}\right)$$

$$= a'_{k-1}\eta_{k-1}+b'_{k+1}\eta_{k+1}-(a'_k+b'_k)\eta_k \tag{A-8}$$

It will be useful to define the variable η_k such that it represents the number density of electrons per unit energy in bin k:

$$\eta_k = \frac{n_k}{\Delta\varepsilon_k} \quad [\mathrm{cm^{-3}eV^{-1}}] \tag{A-9}$$

Doing so will allow the following expressions to be redefined as

$$\overline{n_k} = \left(\frac{n_{k+1}}{\Delta\varepsilon_{k+1}} + \frac{n_k}{\Delta\varepsilon_k}\right)\frac{\Delta\varepsilon_k}{2} \tag{A-10a}$$

$$\frac{\partial n_k}{\partial\varepsilon} = \eta_{k+1} - \eta_k \tag{A-10b}$$

The motivation for doing this lies in the fact that the electron number density in each energy bin needs to be weighted by the width of that bin. Using Eq (A-10a) and (A-10b), $J_f(k)$ can be expressed as

$$J_f(k) = \alpha_k\left[(\eta_{k+1} + \eta_k)\frac{\Delta\varepsilon_k}{4} - \varepsilon_k(\eta_{k+1} - \eta_k)\right]$$

$$\text{where} \quad \alpha_k = \frac{2e^2N^2(E/N)^2}{3m_e\nu_k} \tag{A-11}$$

In a like manner, $J_f(k-1)$ can be written as

$$J_f(k-1) = \alpha_{k-1}\left[(\eta_k + \eta_{k-1})\frac{\Delta\varepsilon_{k-1}}{4} - \varepsilon_{k-1}(\eta_k - \eta_{k-1})\right] \tag{A-12}$$

Substituting Eq (A-11) and (A-12) into Eq (A-8), and grouping into like terms of η_k, η_{k+1}, and η_{k-1}, the coefficients can be written as

$$b'_f(k+1) = \frac{\alpha_k}{\Delta\varepsilon_k}\left(\varepsilon_k - \frac{\Delta\varepsilon_k}{4}\right)$$

$$a'_f(k) = \frac{\alpha_k}{\Delta\varepsilon_k}\left(\frac{\Delta\varepsilon_k}{4} + \varepsilon_k\right) \qquad \text{(A-13)}$$

where the prime designates that these are the coefficients for the η_{k+1} and η_k terms respectively.

Flux due to Elastics

Rockwood gives the electron current density in energy space due to elastic energy transfer as

$$J_{el} = \bar{\nu}\left[n\left(\frac{kT}{2} - \varepsilon\right) - kT\varepsilon\frac{\partial n}{\partial\varepsilon}\right] \qquad \text{(A-14)}$$

The finite differenced expression of Eq (A-14) as given by Rockwood (14:2349) allowed A_k's that could be negative, thus causing numerical instabilities in the computation of the solution. Following the guidelines of Greene (7:2948), the following approach is used:

$$J_{el} = \frac{\bar{\nu}nT}{2} - n\varepsilon\bar{\nu} - \bar{\nu}T\varepsilon\frac{\partial n}{\partial\varepsilon} \qquad \text{(A-15)}$$

where to represent $-\partial J_{el}/\partial\varepsilon$ the first term of Eq (A-15) is backward differenced, the second term is forward differenced, and the last is backward differenced. Thus, the following expressions are used:

$$-\frac{1}{2}\partial\frac{\bar{\nu}nT}{\partial\varepsilon} = -\frac{T}{2}[\bar{\nu}_k\eta_k - \bar{\nu}_{k-1}\eta_{k-1}] \quad \text{(A-16a)}$$

$$\frac{\partial(n\varepsilon\bar{\nu})}{\partial\varepsilon} = [\bar{\nu}_{k+1}\varepsilon^+_{k+1}\eta_{k+1} - \bar{\nu}_k\varepsilon^+_k\eta_k] \quad \text{(A-16b)}$$

$$\frac{\partial}{\partial\varepsilon}\left[\bar{\nu}T\varepsilon\frac{\partial n}{\partial\varepsilon}\right] = T[\bar{\nu}_k\varepsilon^+_k\left(\frac{\eta_{k+1}-\eta_k}{\Delta\varepsilon_k}\right) - \bar{\nu}_{k-1}\varepsilon^+_{k-1}\left(\frac{\eta_k-\eta_{k-1}}{\Delta\varepsilon_k}\right)]$$

$$\text{where} \quad \varepsilon^+_k = \varepsilon_k - \frac{\Delta\varepsilon_k}{2} \quad \text{(A-16c)}$$

Again, grouping into like terms of η_k, η_{k+1}, and η_{k-1}, the coefficients can be written as

$$a_{el}'(k+1) = \bar{\nu}_{k+1}\varepsilon^+_{k+1} + \frac{T\bar{\nu}_k\varepsilon^+_k}{\Delta\varepsilon_k} \quad \text{(A-17b)}$$

$$a_{el}'(k) = \bar{\nu}_k T\left[\frac{1}{2} + \frac{\varepsilon^+_k}{\Delta\varepsilon_k}\right] \quad \text{(A-17a)}$$

where the prime designates that these are the coefficients for the η_{k+1} and η_k terms respectively.

Putting it all together

Moving back to the original representation for n_k and n_{k+1}, the coefficients become

$$a(k) = \frac{2e^2E^2}{3m_e\nu_k}\left(\frac{\Delta\varepsilon_k}{4} + \varepsilon_k\right)\left(\frac{1}{\Delta\varepsilon_k}\right)^2 + \frac{\bar{\nu}_k T}{2\Delta\varepsilon_k}\left[1 + \frac{2\varepsilon^+_k}{\Delta\varepsilon_k}\right] \quad \text{(A-18a)}$$

$$b(k+1) = \frac{2e^2E^2}{3m_e\nu_k}\left(\varepsilon_k - \frac{\Delta\varepsilon_k}{4}\right)\left(\frac{1}{\Delta\varepsilon_k}\right)\left(\frac{1}{\Delta\varepsilon_{k+1}}\right) + \frac{\bar{\nu}_{k+1}\varepsilon^+_{k+1}}{\Delta\varepsilon_{k+1}} + \frac{T\bar{\nu}_k\varepsilon^+_k}{\Delta\varepsilon_k\Delta\varepsilon_{k+1}} \qquad \text{(A-18b)}$$

In practice, it has been found that the use of these equations for the case of a zeroed electric field results in the distribution obtaining the Maxwellian steady state solution as expected. In these cases, it has been verified that the average energy of the distribution is 3/2 the gas temperature. However, when Eq (17a) adn (17b) are used in conjunction with a non-zero electric field, the B_k coefficients, which govern the rate of demotion from one bin to the next lower bin, are too large, and result in a distribution which falls off much faster than it should. Therefore, in the present version of Megaboltz, the Rockwood recoil expressions rederived for the non-uniform energy axis are used when an electric field is present, while Eq (17) is used with no electric field present. The Rockwood recoil term is Eq (15a) expressed as

$$J_{el} = \bar{\nu}\left[n\left(\frac{T}{2} - \varepsilon\right) - T\varepsilon\frac{\partial n}{\partial\varepsilon}\right] \qquad \text{(A-19)}$$

Again using Eq (A-10a) and (A-10b), this equation can be finite differenced according to Eq (A-9). Collecting the coefficients of like electron number density (n_{k-1}, n_k, n_{k+1}), the terms for a_{k-1}, $(a_k + b_k)$, and b_{k+1} are established. The resulting expressions are given as

$$a_{el}(k) = \frac{\bar{\nu}_k}{\Delta\varepsilon_k}\left[\frac{T}{\Delta\varepsilon_k}\left(\varepsilon_k + \frac{\Delta\varepsilon_k}{4}\right) - \frac{\varepsilon_k}{2}\right] \qquad \text{(A-19a)}$$

$$b_{el}(k+1) = \frac{\bar{\nu}_k}{\Delta\varepsilon_{k+1}}\left[\frac{T}{\Delta\varepsilon_k}\left(\varepsilon_k - \frac{\Delta\varepsilon_k}{4}\right) + \frac{\varepsilon_k}{2}\right] \qquad \text{(A-19b)}$$

Appendix B

Derivation of electron-electron collision term for a non-uniform energy axis

Let an energy axis be defined such that the energy of bin k, ε_k, is defined at the center of the bin with a width $\Delta\varepsilon_k$. Using this definition, n_k represents the number density of electrons with energy between $\varepsilon_k - \frac{\Delta\varepsilon_k}{2}$ and $\varepsilon_k + \frac{\Delta\varepsilon_k}{2}$. The time rate of change of the electron number density at ε_k is given by

$$-\frac{\partial J_{ee}}{\partial \varepsilon}\Big|_{\varepsilon=\varepsilon_k} = -\frac{J_{k+1/2} - J_{k-1/2}}{\Delta\varepsilon_k}$$

$$= a'_{k-1} n_{k-1} + b'_{k+1} n_{k+1} - (a'_k + b'_k) n_k \qquad \text{(B-1)}$$

Now, let the electron number density at the boundary between two bins to defined as

$$n\Big|_{\varepsilon=\varepsilon_{k+1/2}} = \frac{\Delta\varepsilon_k n_{k+1} + \Delta\varepsilon_{k+1} n_k}{\Delta\varepsilon_k + \Delta\varepsilon_{k+1}} \qquad \text{(B-2)}$$

Similarly, the energy derivative of the electron number density at the boundary is defined as

$$\frac{\partial n}{\partial \varepsilon}\Big|_{\varepsilon=\varepsilon_{k+1/2}} = \frac{n_{k+1} - n_k}{\varepsilon_{k+1} - \varepsilon_k} \qquad \text{(B-3)}$$

Eq (7) is finite differenced at the boundary of the bins k and k+1, thus becoming

$$J_{k+1/2} = \alpha\left\{\left(\frac{P_{k+1} + P_k}{2}\right)\left[\frac{1}{2\varepsilon_{k+1/2}}\left(\frac{\Delta\varepsilon_k n_{k+1} + \Delta\varepsilon_{k+1} n_k}{\Delta\varepsilon_k + \Delta\varepsilon_{k+1}}\right) - \left(\frac{n_{k+1} - n_k}{\varepsilon_{k+1} - \varepsilon_k}\right)\right]\right.$$

$$\left. - \left(\frac{Q_{k+1} + Q_k}{2}\right)\left(\frac{\Delta\varepsilon_k n_{k+1} + \Delta\varepsilon_{k+1} n_k}{\Delta\varepsilon_k + \Delta\varepsilon_{k+1}}\right)\right\} \qquad \text{(B-4)}$$

A similar differencing at the boundary of bins k and k-1 results in

$$J_{k-1/2} = \alpha\{\left(\frac{P_k + P_{k-1}}{2}\right)\left[\frac{1}{2\varepsilon_{k-1/2}}\left(\frac{\Delta\varepsilon_{k-1}n_k + \Delta\varepsilon_k n_{k-1}}{\Delta\varepsilon_{k-1} + \Delta\varepsilon_k}\right) - \left(\frac{n_k - n_{k-1}}{\varepsilon_k - \varepsilon_{k-1}}\right)\right]$$

$$- \left(\frac{Q_k + Q_{k-1}}{2}\right)\left(\frac{\Delta\varepsilon_{k-1}n_k + \Delta\varepsilon_k n_{k-1}}{\Delta\varepsilon_{k-1} + \Delta\varepsilon_k}\right)\} \qquad \text{(B-5)}$$

Replacing the integrals contained in Eq (7) with summations,

$$P_k = 2\sum_{l=1}^{S}[\varepsilon_k^{-1/2}\varepsilon_l n_l \Delta\varepsilon_l H_{k,l}$$

$$+ \varepsilon_k\varepsilon_l^{-1/2} n_l \Delta\varepsilon_l (1 - H_{k,l})] \qquad \text{(B-6)}$$

$$Q_k = 3\varepsilon_k^{-1/2}\sum_{l=1}^{S} n_l \Delta\varepsilon_l H_{k,l} \qquad \text{(B-7)}$$

$$\text{where } H_{k,l} = \begin{cases} 0 & l > k \\ 1 & l \le k \end{cases}$$

Substituting Eq (B-6) and (B-7) into (B-5), and collecting the coefficient of n_{k-1}, a_{k-1} as used in Eq (B-1) is determined. This coefficient becomes

$$a_{k-1} = \sum_{l=1}^{S} \alpha n_l \frac{\Delta\varepsilon_l}{\Delta\varepsilon_k}\{(\varepsilon_k^{-1/2}H_{k,l} + \varepsilon_{k-1}^{-1/2}H_{k-1,l})$$

$$\times \left[\varepsilon_l u_{k-1} - \frac{3}{2}\left(\frac{\Delta\varepsilon_k}{\Delta\varepsilon_{k-1} + \Delta\varepsilon_k}\right)\right]$$

$$+ [\varepsilon_k(1 - H_{k,l}) + \varepsilon_{k-1}(1 - H_{k-1,l})](\varepsilon_l^{-1/2}u_{k-1})\}$$

$$\text{where } u_{k-1} = \frac{1}{2\varepsilon_{k-1/2}}\left(\frac{\Delta\varepsilon_k}{\Delta\varepsilon_{k-1} + \Delta\varepsilon_k}\right) + \frac{2}{\Delta\varepsilon_{k-1} + \Delta\varepsilon_k} \qquad \text{(B-8)}$$

Defining a'_{k-1} such that

$$a'_{k-1} = \sum_{l=1}^{S} A_{k-1,l} n_l \tag{B-9}$$

the coefficient $A_{k,l}$ is written as

$$\begin{aligned} A_{k,l} = \alpha \frac{\Delta\varepsilon_l}{\Delta\varepsilon_k} \{ & (\varepsilon_{k+1}^{-1/2} H_{k+1,l} + \varepsilon_k^{-1/2} H_{k,l}) \\ & \times \left[\varepsilon_l u_k - \frac{3}{2} \left(\frac{\Delta\varepsilon_{k+1}}{\Delta\varepsilon_k + \Delta\varepsilon_{k+1}} \right) \right] \\ & + [\varepsilon_{k+1}(1 - H_{k+1,l}) + \varepsilon_k (1 - H_{k,l})] (\varepsilon_l^{-1/2} u_k) \} \end{aligned} \tag{B-10}$$

This coefficient for n_k can be interpreted as the rate at which electrons with energy ε_k are promoted to energy ε_{k+1}. This promotion is accomplished by an electron with energy ε_l being demoted to energy ε_{l-1}. An expression similar to Eq (B-10) can be derived as the coefficient of n_{k+1} by using Eq (B-4). When transformed into the k^{th} bin, this coefficient becomes $B_{k,l}$, and is interpreted as the rate at which electrons with energy ε_k are demoted to energy ε_{k-1} by electrons with energy ε_l going to ε_{l+1}.

Boundary conditions are applied to Eq (B-10) and the corresponding equation for $B_{k,l}$ so that conservation of particles is strictly observed. These boundary conditions given by Eq (38), and physically mean that no electron can be demoted from the lowest energy bin when $k = 1$, or promoted from the highest energy bin when $k = S$. When Eq (B-10) and the corresponding equation for $B_{k,l}$ are programmed, energy is not conserved. Additionally, these coefficients will not drive the distribution toward a Maxwellian over time as they should when only electron - electron collisions are considered. In order for the solution method to strictly observe these last

two properties, the $A_{k,l}$'s and $B_{k,l}$'s must be properly constructed.

Conservation of energy can be expressed as

$$\frac{d}{dt}\left[\frac{\int_0^\infty \varepsilon n(\varepsilon)d\varepsilon}{\int_0^\infty n(\varepsilon)d\varepsilon}\right] = \frac{\sum_{k=1}^{S} \varepsilon \frac{dn_k}{dt}\Delta\varepsilon_k}{\sum_{k=1}^{S} n_k\Delta\varepsilon_k} = 0 \qquad \text{(B-11)}$$

Using Eq (B-1) as the time derivative of the electron number density, and the definitions of the coefficients a'_{k-1}, a'_k, b'_k, and b'_{k+1}, as given by Eq (37), Eq (B-11) becomes

$$\sum_{k,l} n_k n_l[(\varepsilon_{k+1}-\varepsilon_k)A_{k,l}-(\varepsilon_k-\varepsilon_{k-1})B_{k,l}] = 0 \qquad \text{(B-12)}$$

This condition will be ensured by

$$B_{k,l} = \left(\frac{\varepsilon_{l+1}-\varepsilon_l}{\varepsilon_k-\varepsilon_{k-1}}\right)A_{l,k} \qquad \text{(B-13)}$$

In order to determine the constraint on the matrices caused by the need to obtain the Maxwellian in the steady state, the microscopic interpretations of $A_{k,l}$ and $B_{k,l}$ are used. Once the steady state Maxwellian has been achieved, then the flux from bin k upward to bin k+1 must be matched exactly by the downward flux from bin k+1 to bin k. Thus,

$$A_{k,l}n_k n_l\left(\frac{\Delta\varepsilon_l}{\Delta\varepsilon_k}\right) = B_{k+1,l-1}n_{k+1}n_{l-1}\left(\frac{\Delta\varepsilon_{l-1}}{\Delta\varepsilon_{k+1}}\right) \qquad \text{(B-14)}$$

Using Eq (B-13) to express $B_{k+1,l-1}$ in terms of the A matrix, Eq (B-14) becomes

$$A_{k,l} = A_{l-1,k+1}\left(\frac{\varepsilon_l - \varepsilon_{l-1}}{\varepsilon_{k+1} - \varepsilon_k}\right)\frac{n_{k+1}}{n_k}\frac{n_{l-1}}{n_l} \tag{B-15}$$

Since the Maxwellian distribution defines the electron number density n_k as

$$n_k = C\varepsilon^{1/2}\exp\left[-\frac{\varepsilon_k}{T}\right] \tag{B-16}$$

the two number density ratios can be rewritten and the final expression for Eq (B-14) becomes

$$A_{k,l} = A_{l-1,k+1}\left(\frac{\varepsilon_l - \varepsilon_{l-1}}{\varepsilon_{k+1} - \varepsilon_k}\right)\left(\frac{\varepsilon_{k+1}}{\varepsilon_k}\right)^{1/2}\left(\frac{\varepsilon_{l-1}}{\varepsilon_l}\right)^{1/2}$$
$$\times \exp\left[\frac{(\Delta\varepsilon_l + \Delta\varepsilon_{l-1}) - (\Delta\varepsilon_{k+1} - \Delta\varepsilon_k)}{2T}\right] \tag{B-17}$$

In practice, Eq (B-10) is used to define the part of the A matrix on and below the diagonal, as well as the elements just above the diagonal. Eq (B-17) is then used to define the rest of the A matrix. The first column and last row of the A matrix is set to zero, which will ensure the conservation of particles as demanded by Eq (38), then the entire B matrix is constructed by the use of Eq (B-13).

Appendix C

User's Guide to MEGABOLTZ

The current version of MEGABOLTZ is designed to run under UNIX version 4.3, with the IMSL v9.2 library and METALIB library installed. There are currently two calls to the IMSL library for the L-U decomposition and substitution, while all graphing functions are accomplished by the METALIB library. In order to run, MEGABOLTZ expects some files to be in the same directory as the executable code. These files consist of the following:

FILE	DESCRIPTION
megaboltz	executable Boltzmann solver code
input.com	ASCII data file describing the physical conditions under the solution is to be obtained
*.crs	ASCII cross section data file. ie., ar.crs for Argon or h2.crs for Hydrogen. This file is explained in detail in Appendix D.

The input file, input.com, is shown in Figure 36. The E/N select switch allows the user to chose if the calculation is for one E/N or for a list of E/N's. If a list of E/N's is used, the list may be either equally spaced (choice 3), or contained in an external file of E/N's called "eovern.dat", (choice 2). If the equally spaced option is used, the number of data points is calculated by [(Start E/N - End E/N) / delta E/N]. For example, suppose you are interested in running 2 to 30 Td, by 2 Td increments. Select the start E/N value to be 30.00d-17, and the end value to be 2.00d-17. The number of datapoints is [(30-2)/2] = 14. Notice that the actual number of datapoints will be one more than this, or 15. The start value is given as 30 Td instead of 2 Td because MEGABOLTZ expects the higher value to be given first. This choice was driven by the quicker convergence at the higher E/N values. The initial guess distribution for the list of E/N's will be a

Maxwellian at the start E/N value. For each next E/N value, the initial guess will be the converged solution for the previous E/N. Doing things in this order speeds the calculation of the distribution at each E/N.

```
*--- Input Parameters
  E/N Select:
   1-Single Point  -> Solve for START E/N value only
   2-Read Ext File -> Solve for E/N's in File 'eovern.dat'
   3-Iterate       -> Solve for equally spaced E/N's below
    START E/N (V-Cm^2): 1.0D-17
     END E/N        : 40.00D-17
     DATA Points    : 8
   ----------------------
   E/N Choice (1,2,3) : 1
   Gas Temperature (K): 3.d2
   Gas Pressure (Torr): 7.6d2
e- Num Density (Cm^-3): 1.0D13

*--- Mesh Parameters
        Time Step (S): 1.d-9
      Number Of Bins: 150
    Bin Width Select:
    1-VARIABLE -> Variable Bin Width
    2-LOG      -> Logarithmic Bin Width
    3-LINEAR   -> Constant Bin Width
      Max Energy (eV): 10.0
    ----------------------
    Bin Width  (1,2,3): 3
*--- Program Switches
 E-E Collisions? (Y/N): N
      e- Beam? (Y/N): N
       Source current: 1.d-3
      Source location: 30.0
       Save Data As: test.dat
       Save Graph As: test.plt
*--- Gasmix data by type (5 maximum), percent (enter as XXX), and whether
    you want to view its cross-sections (enter either Y or N)
_Gas_ _Percent__View?_
ar       99.9      N
f        0.1       N
EOF      0.0       N
```

Figure 36. Sample Input File "input.com" for MEGABOLTZ

The mesh parameters determine the energy grid along which the solution will be determined. For a uniform grid, the number of energy bins and the maximum energy will determine the energy bin width. In the case of a Log grid, this maximum energy has no meaning. Instead, the program will prompt the user for an alpha value (Eq (64)). The maximum energy is determined by the sum of each energy bin defined by this parameter. By varying alpha, the maximum energy can be selected. The code will loop through this process until the user agrees to procede with the resulting maximum energy. The Variable grid allocation method is presently under development, and its use is presently not recommended. The time scale to be used is also set in this block. This sets the time step of integration for the coupled set of differential equations, given in Eq (11) and Eq (23). This value should be at least as small as the characteristic time scale for electron interaction, given by $1/\nu$, where ν is the collisional frequency for the dominate process.

The file names under which the data and graphs should be saved are listed in the next block, along with the swithes governing electron-electron collisions and electron beams. If a duplicate file name is used, MEGABOLTZ will prompt the user for a new file name. The final block lists the gases to include in the calculation. The gases listed in this section must be spelled exactly as the prefix to the .crs extension for the corresponding gas. For example, if the cross section file is ar.crs, then the gas listed here is ar, not Ar. After the final gas, EOF must be placed as the end of file marker, along with a gas concentration of 0.0%. This an important step, because without it MEGABOLTZ may be able to compute a converged solution that is incorrect.

Once the solution has converged, MEGABOLTZ will save all the transport and energy balance data to the file specified in "input.com". The solution will be saved in a file named "N.dat". The graph of this file will be saved to the file specified in "input.com". A listing of all files written by MEGABOLTZ is shown below.

FILE	DESCRIPTION

test.dat	Name of ASCII file specified by user in "input.com" containing transport and energy balance data for each E/N calculation.
test.plt	Name of file specified by user in "input.com" containing the plot file of the distribution. This file is constructed so as to print out on a laser printer when used with the command mit "test.plt" > lpr -Pimagen, from the Unix sytem prompt.
N.dat	Name of ASCII file containing the electron energy distribution of the converged solution for each energy bin.
xsmod.dat	Name of ASCII file containing cross section information. This file is written as each data point from the cross section file *.crs is read. It is used mainly for debugging *.crs files. (Appendex D)

The sample output file "test.dat" is shown below:

```
 Megaboltz Output Data
 Bins  Binwidth  Timestep
 150  0.1000   1.00E-09
 N1/N   :  0.00E+00
 Ne final:  8.75437E+12
  E/N        Rion       Rion2      Rexc       Rsuper     Rattach
1.0000E-16 1.2312E-17 0.0000E+00 5.9674E-12 0.0000E+00 0.0000E+00
  E/N        <E>     E char      Vd         Df       E Balance
 1.000D-16  5.371D+00  7.819D+00  9.221D+05  2.946D+03  3.784D-01
  Megaboltz Energy Calculations
  Energy Loss Mechanisms
E/N        Sys Loss   El Losses  Exc Losses  Ion Losses  Atch Losses
1.0000E-16 2.2655E+09 6.2973E+08 1.7045E+09 3.259E+04  0.0000+00
  Energy Gain Mechanisms
E/N        Sys Gains  J.E        Super      e Beam
1.0000E-16 2.2569E+09 2.2569E+09 0.0000E+00 0.0000E+00
```

Figure 37. Sample Output File "test.dat" From MEGABOLTZ

Finally, it must be stressed that MEGABOLTZ expects the parameters listed in "input.com" to be in the proper place. If the template given for "input.com" is followed exactly, no problems will occur. However, MEGABOLTZ has not been "idiot-proofed", and it is adviseable to keep a backed up copy of this file. Even experienced users have found it to be advantageous.

Appendix D

Cross Section Format for Megaboltz

Just as MEGABOLTZ expects the "input.com" file to properly formatted, it expects each cross section file to be properly formatted. The purpose of this appendex is to familiarize the user with the construction of the cross section file to the extent that modification can be completed relatively painlessly. Again, having a backed up copy of each cross section file is an extremely good idea. Figure 38 shows the cross section data file for Argon.

The first line gives just the gas name. This title is not read by MEGABOLTZ, so it can be in any format. The next line contains three pieces of information. The first four spaces are dedicated to the molecular weight for the gas, while the next three are used to designate how many cross sections are included in the file. This must be an integer between 1 and 999 (which would be a lot of cross sections!). The last number is the ionization threshold in eV for the gas, however it is not read by MEGABOLTZ. Each line is ended by a forward slash (/) that must be outside of the defined block area.

Each cross section table within the cross section file consists of three "lines", except the first table which is the momentum transfer table and consists on only two "lines". These lines are not to be confused with lines of ASCII, but rather have no particular maximum length. The end of one of these line is defined by a forward slash (/). The first line of each table begins with a three space block dedicated to the number of data point pairs (energy, cross section) in the table. The number occupying this block must be an integer. The next 12 spaces are in a reserved block which designates the type of process the table contains. For example, this identifier could be "elastic", "inelastic", "ionization", or "attachment", where the quote marks are not used. In the process of running, MEGABOLTZ will look for these identifying words as labels, thus they must be spelled correctly, with no capitals. The next 15 spaces are dedicated to a block that describes the origin of the data. The quotes are included as part of the 15 total spaces of the block. The

next 15 spaces are dedicated to another block, which can be used as a continuation of the previous one. Again, the quotes are included as part of the 15 space total. The final variable on this line represents the scale of the data points. This occupies 4 spaces (XXX.X). This is used as a multiplier for the cross sectional values, and is usually 1.0. This line is ended with a forward slash (/) that is outside of the defined block area, however, remember that Fortran 77 can only read 72 characters per line.

```
AR
 40. 5  15.759 /
54 elastic   'FAUST.J.PHYS,''1977,30,61-72' 1.0 /
0.000,0.000 0.014,3.880 0.017,3.560 0.020,3.280 0.025,2.890
0.030,2.570 0.035,2.290 0.040,2.050 0.050,1.662 0.060,1.357
0.070,1.114 0.080,0.916 0.090,0.754 0.100,0.621 0.110,0.511
0.120,0.420 0.130,0.348 0.140,0.284 0.150,0.233 0.170,0.161
0.180,0.135 0.190,0.115 0.200,0.101 0.210,0.092 0.220,0.086
0.230,0.085 0.240,0.087 0.050,0.091 0.260,0.098 0.280,0.120
0.300,0.151 0.320,0.188 0.325,0.206 0.400,0.317 0.500,0.504
0.650,0.792 0.800,1.050 1.000,1.370 1.200,1.660 1.500,2.050
1.700,2.330 2.000,2.700 2.500,3.430 3.000,4.200 4.000,5.700
5.000,7.600 7.600,12.50 10.00,16.61 15.00,16.14 20.00,12.50
40.00,6.0   60.00,4.6   80.00,4.1   100.00,4.0   /
27 inelastic  'AR E1'      '          ' 1.0  /
0.    , 0.     11.6  , 0.    11.65  , .0037
11.7  , .0074  11.75 , .0104 11.8   , .0134
11.85 , .0141  11.9  , .0149 12.    , .0163
12.1  , .0168  12.2  , .017  12.4   , .018
12.6  , .0188  12.8  , .0196 13.    , .0205
13.2  , .0213  13.4  , .022  14.    , .0225
20.   , .0271  30.   , .0275 40.    , .0275
50.   , .0233  60.   , .0203 70.    , .0181
80.   , .0163  90.   , .0149 100.   , .0137
11.6, 1.0, 0.0 /
23 inelastic 'AR E2'      '          ' 1.0   /
0.    , 0.     11.8  , 0.    11.85  , .0022
11.9  , .0078  12.   , .0134 12.1   , .0172
12.2  , .0214  12.4  , .0295 12.6   , .0411
12.8  , .0516  13.   , .0643 13.2   , .0753
13.4  , .0778  13.6  , .078  14.    , .0784
30.   , .0944  40.   , .0912 50.    , .0774
60.   , .0675  70.   , .0600 80.    , .0542
90.   , .0494  100.  , .0455  /
11.8, 1.0, 0.0 /
24 inelastic  'AR E3'      '          ' 1.0  /
0.    , 0.     13.2  , 0.    13.4   , .0013
13.5  , .0018  13.6  , .0069 13.7   , .0133
13.8  , .0206  14.   , .0359 15.    , .1323
16.   , .2826  17.   , .465  18.    , .645
```

```
19.   , .82   20.   , 1.16  22.   , 1.27
26.   , 1.48  30.   , 1.56  40.   , 1.48
50.   , 1.256 60.   , 1.095 70.   , .9740
80.   , .8790 90.   , .8024 100.  , .7390 /
13.2, 1.0, 0.0 /
38 ion      'AR I'      'KIEFFER,78'   1.0  /
0.    , 0.    15.759 , 0.     16.   , .02023
17.   , .1337 18.   , .2938  19.   , .4601
20.   , .6272 21.   , .7873  22.   , .9325
23.   , 1.056 24.   , 1.179  25.   , 1.302
26.   , 1.408 28.   , 1.601  30.   , 1.803
32.   , 1.962 34.   , 2.111  36.   , 2.243
38.   , 2.331 40.   , 2.393  42.5  , 2.446
45.   , 2.49  50.   , 2.534  55.   , 2.595
60.   , 2.657 65.   , 2.727  70.   , 2.771
75.   , 2.815 80.   , 2.841  85.   , 2.85
90.   , 2.859 100.  , 2.85   115.  , 2.824
130.  , 2.762 145.  , 2.709  160.  , 2.622
180.  , 2.516 200.  , 2.393  /
15.759 , 1.0/
--EOR--
--EOF--
```

Figure 38. Cross Section Data File for Argon

The second line of each table actually consists of many lines of numbers, representing the pointwise description of the cross section. These data points are formatted as (Energy, Cross section), where the energy is in units of eV, and the cross section default is units of 10E-16 cm^2. This default can be modified with the scale variable defined earlier. There is a comma between each number of the data pair, while at least one space separates each data pair from each other. Once each of the data pairs in each table is listed, a forward slash (/) designates the end of the line.

The third line is included only for cross section tables after the momentum transfer table. The format of this third line depends on whether the table is for an "inelastic" process or not. If the table is for "inelastic", then the third line consists of three blocks. If the table is for "ionization" or "attachment", then this third line is constructed of only two blocks. Each of these blocks has no specific length, rather, they are separated by commas. The first block of both types of lines designates the threshold energy for the process, in eV. The second number in the third line rep-

resents the ratio of the number of gas particles to be affected by the process to the number of gas particles in the ground state. Thus, this number must be between 0.0 and 1.0. When this number is multiplied by the total number of gas molecules, the result is the number of molecules affected by the state. For any process affecting ground state molecules, this number will be 1.0. This includes ground state ionization and excitation, as well as a process such as attachment. By making the value of this variable 0.0 for any of these processes, that particular process can be "turned-off" in this manner. For "inelastic" processes, the third number designates the number of superelastic molecules to consider. This number is a ratio of the number of molecules in the upper excited state of the excitation process, to the number in the lower state of the same process. Consider an excitation process from the ground state to some upper excited state j. If only 1 out of every 10,000 molecules is in the state j, then this number would be 1.0E-5. In calculating the effects of superelastic collisions, the code will use this number in determining the number of collisional partners for the electrons. This line is ended with a forward slash (/).

The selection of these parameters formatted in this manner may seem to be ackward, but after practice their use will become second nature and comfortable. The hard structure of the cross section files is very strict, and very unforgiving. In order to help the user with the formatting of the files, MEGABOLTZ will recreate the cross section file as it reads it. This file, called "xsmod.dat", is created each time MEGABOLTZ runs, and does not have to be in existence prior to running the code. This file actually contains two files: the first file is the cross section file rewritten, while the second file consists of the interpolated cross sections for up to five tables. Many times MEGABOLTZ errors can be traced to incorrectly formatted cross section files. "xsmod.dat" is designed to help iron out these errors.

BIBLIOGRAPHY

1. Bretagne, J. et al, "On Electron Energy Distribution Functions in Low-Pressure Magnetic Multicusp Hydrogen Discharges", Journal of Physics D: Applied Physics, 19:1197-1211 (1986).
2. Bretagne, J. et al, "Low-Energy Electron Distribution in an Electron-Beam Generated Argon Plasma", Journal of Physics D: Applied Physics, 15:2205-2225 (1982).
3. Bretagne, J., et al., "Electron Energy Distributions in Electron-Beam-Sustained Discharges: Application to Magnetic Multicusp Hydrogen Discharges", Journal of Physics D: Applied Physics, 18:811-825 (1985).
4. Cherrington, B.E. Gaseous Electronics and Gas Lasers.
5. Dutton,J. "A Survey of Electron Swarm Data", Journal of Chemistry and Physics, 4:577-777 (1975).
6. Elliott, C.J. and A.E. Greene, "Electron Energy Distributions in e-Beam Generated Xe and Ar Plasmas", Journal of Applied Physics, 47:2946-2953 (July 1976).
7. Greene, A.E. Memorandum for Record, 8 May 1975.
8. Holstein, T., "Energy Distribution of Electrons in High Frequency Gas Discharges", Physical Review, 70:367-384 (1946).
9. Honey, D.A. A Numerical Solution to the Boltzmann Equation for Use in Calculating Pumping Rates in a CO_2 Discharge Laser. MS Thesis, AFIT/GEP/ENP/89D-5. School of Engineering, Air Force Institute of Technology (AU), Wright-Patterson AFB OH, December, 1989.
10. Long, W.H., et al, "Electron Drift Velocities in Molecular-Gas-Rare-Gas Mixtures", Physical Review A, 13:471-475 (1976).
11. Nickel, G.H., "Transport of Spectral Line Radiation in Cylindrical Plasmas"
12. Press, W.H. et al. Numerical Recipes. New York: Cambridge University Press, 1989.
13. Proctor, W.A. and G.H. Canavan. Electron Energy Distribution Functions, Transport Coefficients, and Pumping Rates for Electrically Excited Mixtures of He, N_2, and CO_2.
14. Rockwood, S.D., "Elastic and Inelastic Cross Sections for Electron-Hg Scattering from Hg Transport Data", Physical Review A, 8:2348-2358 (1973).
15. Rozenberg, et al, "On the Possibility of Steady State Negative Mobility in Externally Ionized Gas Mixtures", Journal of Physics D: Applied Physics, 21:1593-1596 (1988).
16. Seger, G.E. A Numerical Solution of the Time-Dependent Boltzmann Equation. MS Thesis, AFIT/GEP/ENP/89D-10. School of Engineering, Air Force Institute of Technology (AU), Wright-Patterson AFB OH, October, 1989.
17. Uman. Introduction to Plasma Physics.
18. Verdeyen, J.T. Laser Electronics. Englewood Cliffs, New Jersey: Prentice-Hall, 1989.
19. Zel'Dovich, Ya.B. and Yu.P. Raizer, Soviet Physics JETP, 20:772 (1965).

20. Hayashi, M. and T. Nimura, "Calculation of Electron Swarm Parameters in Flourine", Journal Applied Physics, 54:4879-4882 (September 1982).

21. Frost, L.S. and A.V. Phelps, "Momentum-Transfer Cross Sections for Slow Electrons in He, Ar, Kr, and Xe from Tranport Coefficients, Physical Review A, 1538-1545 (December 1964).

Vita

Captain William M. Hilbun was born on 12 September 1962, at Columbus Air Force Base, Mississippi. He graduated from Tupelo High School, Tupelo, Mississippi in 1981. He entered the United States Air Force Academy in June 1981, as part of the twenty-seventh class. Upon graduation in May 1985, He received his commission as a Second Lieutenant in the United States Air Force and a Bachelor of Science degree in Physics. He was assigned to the 3246th Test Wing, Munitions Systems Division, Air Force Systems Command, Eglin Air Force Base, Florida. He served there as an Infrared Test Engineer until entering the School of Engineering, Air Force Institute of Technology, in May 1989. Graduating in December 1990, Captain Hilbun received the degree of Master of Science in Engineering Physics. He was reassigned to Foreign Technology Division, Air Force Systems Command, Wright-Patterson Air Force Base, Ohio.

REPORT DOCUMENTATION PAGE

Form Approved
OMB No. 0704-0188

1. AGENCY USE ONLY (Leave blank)	2. REPORT DATE	3. REPORT TYPE AND DATES COVERED
	November 1990	Master's Thesis

4. TITLE AND SUBTITLE
Electron Kinetic Studies Utilizing the Solution of the Time-Dependent Collisional Boltzmann Equation

5. FUNDING NUMBERS

6. AUTHOR(S)
William M. Hilbun, Captain, USAF

7. PERFORMING ORGANIZATION NAME(S) AND ADDRESS(ES)
Air Force Institute of Technology, WPAFB, OH 45433-6583

8. PERFORMING ORGANIZATION REPORT NUMBER
AFIT/GEP/ENP/90D-1

9. SPONSORING/MONITORING AGENCY NAME(S) AND ADDRESS(ES)

10. SPONSORING/MONITORING AGENCY REPORT NUMBER

11. SUPPLEMENTARY NOTES

12a. DISTRIBUTION/AVAILABILITY STATEMENT
Approved for Public Release; Distribution Unlimited

12b. DISTRIBUTION CODE

13. ABSTRACT (Maximum 200 words)

In a continuing effort to analyze plasmas generated in a variety of ways, several refinements and improvements have been added to a numerical solution of the time-dependent collisional Boltzmann equation. The computational method utilized is based on the Rockwood[1] formalism, and includes elastic collisions, excitation, ionization, and supereleastic collisions from multiple states. Attachment is also included. A non-uniform energy grid is incorporated into the method of solution, requiring new finite differenced representations for the electron flux terms from field, recoil, and electron-electron interactions. All of these terms are tested independently and validated against analytic results. Implementation, complete with inelastic collisions, is validated against experimental transport data for both molecular and rare gases. A method for dynamically allocating the energy grid in an effort to optimize the computation is developed and evaluated. The inclusion of the non-uniform grid results in the consideration of larger energy ranges than previously possible.

1. Rockwood, S.D. Physical Review A, 1973 (2348-2358).

14. SUBJECT TERMS
Boltzmann equation, Transport parameters, attachment, electron beams, negative mobility, distribution functions (EEDF)

15. NUMBER OF PAGES
123

16. PRICE CODE

17. SECURITY CLASSIFICATION OF REPORT	18. SECURITY CLASSIFICATION OF THIS PAGE	19. SECURITY CLASSIFICATION OF ABSTRACT	20. LIMITATION OF ABSTRACT
Unclassified	Unclassified	Unclassified	UL